acp-2018-759-RC1
Response to Referee #2

Referee Comment 1: The authors describe the observations and the conditions under which the laminations have been observed, and briefly describe other observations of laminated aerosol and cloud structures.They offer little in the way of explanation for the observed phenomena, however, which seems to me a major shortcoming that should be rectified before publication in Atmospheric Chemistry and Physics.

Author response:

Some proposed explanations for the observed cloud laminations have now been added to the manuscript.

Change to manuscript:

We have added a new Section 5.6 to the manuscript: "Suggested explanations for the laminated phenomena".

New references:

[Beals2015CloudHolography]
Beals, M. J., Fugal, J. P., Shaw, R. A., Lu, J., Spuler, S. M., and Stith, J. L.: Holographic measurements of inhomogeneous cloud mixing at the centimeter scale, Science, 350, 87 – 90, 2015.

[Hocking2001GravityWavesWebsite]
Hocking, W. K.: Buoyancy (gravity) waves in the atmosphere,
http://www.physics.uwo.ca/~whocking/p103/grav_wav.html, 2001.

[Mahrt2014StablyStratBoundaryLayers]
Mahrt, L.: Stably Stratified Atmospheric Boundary Layers, Annual Review of Fluid Mechanics, 46, 23–45, 2014

Referee Comment 2: The figures showing range-scaled photocounts on log scales are a little hard to interpret. How deep are the laminations/striations? Are they closer to 10% or 90% of the total backscatter? More quantitative information would help the reader consider the possible roles of cloud vs interstitial aerosol particles.

Author response:

Examining Figure 2, blue curve, gives a few calculable examples. Let's consider by how many percent of the range-scaled photocounts the in-between layers (yellow in Fig 1) drop the signal compared to the values in the layers themselves (red/orange in Fig 1):

One of the "deeper" laminations gives a result of ((10^9.316 - 10^8.833)/(10^9.316))X100% = 67.11%, while the shallower laminations produce results such as ((10^9.312 - 10^9.103)/(10^9.312))X100% = 38.2%.

These are fairly representative values. Therefore the range-corrected signal drops by between about

35% and 70% of maximum local value between layers.

Change to manuscript:

The text in bold is added to the end of the paragraph on Page 2 lines 15-18 : ``Figure 2 shows selected profiles of range-scaled 532 nm photocounts from Fig. 1 as a function of altitude for four consecutive minutes just after 06:40 UTC, each offset by 1x10^0.6 along the x-axis, between the altitudes of 3 to 4 km. There are clearly horizontal coherent structures in the cloud in space (aliased to time by motion over the lidar) at least down to the 7.5m height resolution of the lidar. **The regions between the laminations generally exhibit range-scaled signals between 35 and 70 % lower than the signals in the laminations immediately above and below."**

Referee Comment 3: To first order, the laminations are reminiscent of the fog striations seen in cold pools under near stable conditions (Stably Stratified Atmospheric Boundary Layers, L. Mahrt, Annual Review of Fluid Mechanics 2014 46:1, 23-45).

Author response:

Thank you for drawing our attention to this publication.

Change to manuscript:

Following Page 5 lines 20-21 "All of the laminated haze layer reports are from aircraft campaigns of short duration, and all excluded from consideration any measurements which included ice crystals and clouds.", we insert a new paragraph:

``In mid-latitude examples of extremely strong atmospheric boundary layer stability, striations of fog may be identified at scales smaller than 1-metre (Mahrt 2014, Fig. 3). These are qualitatively similar to the cloud laminations identified by CRL. Perhaps the two phenomena share similar properties, particularly in terms of the factors which enable the laminations/striations to persist."

Text referring to Mahrt 2014 is also added to the new Section 5.6 ``Suggested explanations for the laminated phenomena." in the response to Reviewer 2 Comment 1, above.

New reference:

[Mahrt2014StablyStratBoundaryLayers]
Mahrt, L.: Stably Stratified Atmospheric Boundary Layers, Annual Review of Fluid Mechanics, 46, 23–45, 2014

Referee Comment 4: What are the wind conditions here? Wind profiles and Richardson numbers would be a useful addition, and potential temperature profiles would also be more instructive that the included temperature profiles.

Author response:

The twice-daily Eureka radiosondes provide windspeed and direction, and we have calculated potential temperature from the sonde temperature profiles as well. These have been added to Figures 5, 7, and 12, with accompanying text.

Richardson numbers (Ri) have not been added to the manuscript. We have calculated Bulk Richardson numbers using radiosonde data, but they are not particularly useful given the scope of this particular paper because the applicability and interpretation of these numbers is nuanced. The issue of turbulence vs. stability could be important, but more specific measurements in this area (e.g. aircraft with a turbulence probe) would be a more appropriate way to study this in detail, in the future.

In general, interpretation of Richardson Numbers smaller than some critical value Rc is that the atmosphere is dynamically unstable and favourable for turbulence, while at values greater than the critical value, it is interpreted to be stably-stratified ("turbulence cannot be sustained", but is also not precluded entirely). The exact Ri values calculated depend on the vertical resolution of the profiles used to make them (Stull 1988, Balsley 2008, Tjernstrom 2009), and so does the value for Rc. Rc can vary from 0.25 (Stull 1988 p. 177) to Rc = 1 or more (Shupe 2017, who uses a minimum cutoff of Ri=1 to guarantee nonturbulence, while still allowing for exceptions of "weak, sporadic" turbulence). The larger Rc values are required for data which is lower resolution and/or smoothed. In our case, if we smooth, or if we choose an inappropriate Rc, we may miss some small patches of instability. This might not be tolerable considering that we are examining laminations at 7.5 m resolution.

As an example, in the figure to the right for 21 March 2017 11:00 UTC, the blue line gives the result at the maximum sonde resolution; the black line gives the result when the windspeed and temperature profiles have been smoothed first by a 3-point moving average filter. We have 238 unsmoothed instances of Ri<1 , and only 139 smoothed instances of Ri<1.

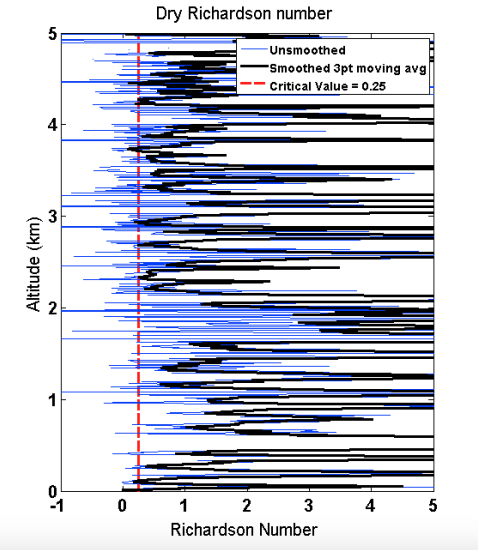

Further, there is a known hysteresis effect in laminar flows, whereby the Richardson Number may begin larger than the critical value (i.e. is stable), then drop below the critical value (there becoming turbulent), and then rise again above the critical value, yet not reaching stability again until a much higher value is reached (Stull 1988 in Brooks 2017). Gravity waves are another example in which turbulence can exist at high Ri. Therefore, interpretation of Ri values we may calculate is also nontrivial.

In order to properly address turbulence/stability, we should also consider whether the dry Ri indicated above are applicable to our situation within clouds. Brooks 2017 advocates the use of such dry Ri (Ri_d; calculated as in Brooks 2017 Eqn 1b, based on Stull 1988 Eqn 5.6.2) only in the case of cloud-free air. They indicate that moist Ri (Ri_m; calculated as detailed in Brooks 2017 Eqn 2, using equations based on Durran&Klemp 1982 Eqn 5) are more appropriate in liquid and mixed phase clouds. To use the latter equations, data contributed from a microwave radiometer or similar is required

- which is far outside the scope of what we can provide for the present manuscript.

Because Richardson Number is a quantity which requires such careful and nuanced calculation and interpretation, the authors did not feel that the current paper was the appropriate place to address into this topic. The Richardson numbers that we calculate at this stage only confound the interpretation of the laminations, while other profiles (wind, temperature, etc) are more straightforward and instructive. To fairly cover the topic of stability would require such space in the paper that it would detract from the main point of the manuscript: the demonstration of laminations within Arctic clouds.

The authors agree that a formal assessment of atmospheric stability in the context of these laminations is an important avenue to pursue in follow-on papers.

New references (just for review response; not required in paper):

[Brooks2017TurbulentSummerBoundaryLayer]
Brooks, I. M., Tjernström, M., Persson, P. O. G., Shupe, M. D., Atkinson, R. A., Canut, G., Birch, C. E., Mauritsen, T., Sedlar, J., and Brooks, B. J.: The turbulent structure of the Arctic summer boundary layer during the Arctic Summer Cloud-Ocean Study, Journal of Geophysical Research: Atmospheres, 112, 9685–9704, 2017.

[Stull1988]
Stull, R. B. (1988). Introduction to Boundary Layer Meteorology (pp. 666). Dordrecht, The Netherlands: Kluwer Academic Publishers.

[Stull2017PracticalMeteorologyBook]
Stull, R.: Practical Meteorology: An Algebra-based Survey of Atmospheric Science, Roland Stull, The University of British Columbia, Vancouver, Canada, 1.02b edn., 2017.

[DurranKlemp1982MoistureBruntVaisala]
Durran, D. R. and Klemp, J. B.: On the Effects of Moisture on the Brunt-Väisälä Frequency, Journal of the Atmospheric Sciences, 39, 2152–2158, 1982.

[Balsley2008GradientRichardsonNumber]
Balsley, B. B., Svensson, G., and Jjernström, M.: On the scale-dependence of the gradient Richardson number in the residual layer, Boundary- Layer Meteorology, 127, 57–72, 2008

[Tjernstrom2009VerticalArcticTropoERA40]
Tjernström, M. and Graversen, R. G.: The vertical structure of the lower Arctic troposphere analysed from observations and the ERA-40 reanalysis, Quarterly Journal of the Royal Meteorological Society, 135, 431–443, 2009.

Change to manuscript:

Figures 5, 7, 12 have been modified to include potential temperature, windspeed, and wind direction plots.

The text fromPage 9 line 30 through Page 10 line 8 (original version numbering), and Page 11 line 9 through Page 11 line 27 (original version numbering), have been changed to address the modified figures.

acp-2018-759-RC2
Response to Referee #1

Major Comments

Referee Comment 1: Figure 2: There appears to be very little attenuation of your light within this cloud. This raises concern for me about multiple scattering enhancing your signal. The Nott et al. 2012 paper described the field of view of the system at 0.3-2mrad. What were you running for this data collection? Is multiple scattering a concern? 3d multiple scattering effects could be very difficult to separate from physical structure and could add (or smooth out) structure on the order of a few range bins depending on the physical features of the cloud.

Author response:

The lidar is run in operational mode at 1.5 mrad field of view.

Test runs with fields of view of 0.5 and 1.0 mrad during the same type of meteorological conditions as those shown in the paper, with laminated clouds extending to about 5 km, have shown that the laminated features remain in the measurements.

The laminated clouds in general are not always particularly optically thick. Therefore, the range-scaled photocount returns are not always much lower at the top edges of the cloud compared to at the lower edges. Recall that all of our plots have been range-scaled. They do attenuate the light overall, as we can see in the 11 November 2017 example: From 1-9:00 UTC, the clear air above the cloud has range scaled count rates < 10^6 MHz m^2. From 9:00-24:00 UTC, the count rates at those altitudes is much higher, at 10^8 MHz m^2.

We do not believe strong multiple scattering to be a major issue here, as the major point of the manuscript concerns the detection of the laminations in the clouds. It is unlikely that the laminations can be explained away by this mechanism.

Multiple scattering is always of concern for any lidar measurement which goes through optically thick clouds. Consider the example from 26 August 2017 (now moved to Appendix ``A summer example of layers on 26 August 2017"; Fig 11), before 4:30 UTC. The optically thick cloud at about 2 km stops nearly all signals from penetrating past that altitude. Multiple scattering would surely be something to concern ourselves with in the upper reaches of the parts of the cloud that we can examine there. Later in that same measurement, after 5:00 UTC, we note that the 2 km cloud has dissipated or moved away, leaving a cloud much thicker in vertical extent, but much thinner in terms of optical properties, for the next hour. Looking above *that* cloud, we again see that the laser beam eventually gets attenuated - but not until 4.5 km or so. We might consider multiple scattering to become important in the upper reaches of the cloud: Particularly later in the measurement, after 6 UTC. That said, it is unlikely that multiple scattering is of considerable concern between 5-6 UTC at the lower altitudes, and there are plenty of laminations present below, say, 3 km. It should be of less concern when the beam penetrates entirely through the cloud without being fully attenuated.

If multiple scattering were present, we would expect its effects to increase (a) with penetration depth into the cloud (because of more integrated material to be scattering off of), and (b) with altitude (because it is geometrically easier to multiply scatter photons in if they originate (originally scatter) farther from our lidar).

A helpful indication that multiple scattering is not the sole cause of these layers is the depolarization measurements. Returns which are multiply scattered would tend to have depolarization parameters (and thus depolarization ratios also) of approximately 1. We do not see any general trends with altitude, nor indeed any positive correlation with overall local count rate, tending toward higher depolarization. Therefore we find that multiple scattering is probably not a major concern for the detection of the laminations in the clouds we observe.

Multiple scattering is something that we can look into more fully in future. Some numerical studies to determine precisely what geometric effects we could expect, for example. Any influence which may yet exist from multiple scattering does not detract from the detection of the laminations in our measurements at their most basic level - it is certainly unlikely that multiple scattering would be accountable for all of the laminations at all altitudes including the lower ones.

Referee Comment 2: You say several times that taking data at lower resolution would cause the thin features to be covered (example on Page 2, Line 19-20). I am skeptical that this would completely remove some of the features you see, though I do not doubt it will change them. For example, the thick count layer at 3km from 4-5.5 UTC in Figure 1 would possibly remain. I believe you should show high vs. degraded resolution to better illustrate this point. Further, it will allow you to quantitatively assess, both what other investigators should be looking for in their lower resolution data and define to what extent data is masked. Specifically, it would help place your work in the context of the previous authors you describe on Page 2, Lines 28-33. Additionally, it will suggest how fruitful further analysis might be, combining data with the low-resolution lidar data products.

Author response:

We will add such a degraded resolution plot to illustrate the point.

Change to manuscript:

We have added a new **Figure 3** to address this. It is comparable to Fig 1 and Fig 2, but shows data at 1 min x 75 m resolution.

Text has been amended to: "If the data are averaged to altitude bins 10 times as large as those shown, all traces of the laminated structure would be erased **(Fig. 3), and the cloud would look more similar to** a smooth cloud."

Referee Comment 3: Why do you not apply overlap corrections? Showing data below 500 meters and not overlap correcting is confusing to me and a bit misleading in places. Suggest either applying the corrections or removing all data below full overlap for clarity.

Author response:

We have removed all lidar data below 500 m. Our overlap correction routines are still in development.

Change to manuscript:

Figures including lidar measurements have been modified to include only data > 500 m. New figures

for quantities unaffected by lidar overlap (e.g. sondes) include all altitudes for context.

Referee Comment 4: Page 10, Lines 27-29 and Figure 3 and Figure 4: Depolarization contours are very noisy. I would argue they are almost unhelpful. In fact, given the results of the McCullough et al. (2018) paper, I am questioning if you have the sensitivity in the depolarization channel to make the described measurements at 1 minute resolution. At the very least, contours of depolarization error bounds should be shown to inform your reader how far they can trust the interpretation of depolarization.

Author response:

We agree that the depolarization results given in this manuscript are noisy, and are not conclusive of much on their own. They are calculated using the d1 method, which uses our low-count rate perpendicular channel, which we would typically run at 20 minute x 37.5 m resolution. To do the d2 method (three-channel) is more difficult to calibrate, and was not done for these dates. Not least because we have realized that there are relevant morphological (and perhaps depolarization-sensitive) features at the highest resolution scales. So to use d1 at low resolution (getting d1 values equal to an average of the layers and inter-layer values, perhaps producing d1 values which do not actually exist anywhere in the cloud!) to calibrate d2... it brings a level of complexity that we could not sufficiently explore given the scope of the current document.

Considering the success we had with the range-scaled photocount profiles at the highest resolutions, we thought it worthwhile to include our d1 values (since we *know* what we're calculating in that instance, although it's noisy) at the same resolution and see what happens.

We might have expected smoother (more uniformly noisy?) d1 colour plots which would have indicated nothing at all. However, as in Fig 4e, we do see that we have enough information to determine (a) no strong correlation of high depolarization with strong laminations (and in fact, anti-correlation seems more likely), and (b) variations in depolarization which do seem to be correlated with fall streaks.

Changes to manuscript:

We have added a new appendix: ``Depolarization Uncertainty", with the following text:

``For completeness, depolarization uncertainties for the two main dates examined in this paper are presented here. Figure 9 for 21 March 2017, and Fig. 10 for 11 November 2017."

Include two new figures **Fig. 9 and Fig. 10.**

In the existing body of the paper:

At page 7 line 9, add the new text: ``**Examples of depolarization parameter plots are Figs. 4e and 6e. Appendix A provides some plots of depolarization uncertainty in Figs. 9 and 10.''**

At Page 10 line 31, add the new text: ``**Although the depolarization plots are somewhat noisy at this resolution, absolute uncertainties are generally between 0.05 and 0.1 (in the same units as depolarization parameter) for the region below 1 km, where the laminations are visible in Fig. 4e. At higher altitudes, uncertainties for this date reach 0.16.''**

At Page 14 line 32, add the new text: ``**For Fig. 6e, the uncertainties are somewhat higher than they are for 21 March 2017 (4e) in regions of high depolarization, reaching values of 0.2 to 0.3 where d>0.5. Similar to the March example, regions on 11 November 2017 in which cloud laminations are visible, namely between 10:30 and 11:00 UTC below 1 km, have absolute uncertainties smaller than 0.06 in general."**

Referee Comment 5: Section 4.3: Perhaps this is best used as an appendix. It is less convincing than the other 2 cases based on the level of information you are able to provide. It might be more helpful to summarize your measurements to describe the percent of time you see clouds with such vertical laminations.

Author response:

We will move this summer example to an appendix. See response to comment 7b in this document about the percentage of time we see clouds with the laminations.

Change to manuscript:

Content from old Section 4.3 has been moved to Appendix C: ``A summer example of layers on 26 August 2017".

Referee Comment 6: Section 5.1-5.3: The discussion in these 3 sections is a major weakness of the paper in my opinion. I do not find the discussion particularly convincing because the topics discussed, while likely being familiar to a reader knowledgeable of lidar hardware, is not particularly well constructed in my opinion.

Author response:

The general construction of this section was dictated by questions that we have received when showing the laminated cloud measurements to colleagues and at conferences. Analagous to R1's Comment 1 ("Could this be a multiple scattering effect?"), the questions addressed in Sections 5.1 - 5.3 show the concerns of those people whose immediate impression is that these laminations might be a result of instrument or measurement effects or artifacts. The authors interpret the laminations to be geophysical, but this is because we have good reasons for believing them not to be instrumental effects, as detailed in this section. Detailed responses follow, but we can be more explicit in the manuscript in explaining why this section exists in the format it does.

Change to manuscript:

Following the sentence "Before attributing the striped effect that we see in our data to geophysical phenomena, we apply due diligence to show that it is not an instrumental effect.", we add the new sentence "**Each of the topics covered by Section 5.1 - 5.4 address a specific instrumental or measurement effect/artifact which has been suggested by members of the broader lidar community as a possible indication that the laminations are not geophysical phenomena.**"

R1 comment 6, continued: My concerns are as follows:

6a) PMT or saturation more generally should serve to smooth your profiles in every case I can imagine. If the section of your glued profile originates from photon counting data, photons will be under-reported and thus thick clouds will seem thinner. If the portion of the profile is from the analog counting system and you are under reporting intensity (or even clipping the ADC), you are operating so far outside of the designed regime of the detectors that the data is likely not valid. Additionally, you claim to have corrected it in Section 3.

Author response:

We have no saturated measurements in the paper. Indeed, as R1 points out, it would not be appropriate to include saturated measurements in our analyses in the first place. One sentence explaining that we are not operating near saturation limits for our system should suffice to stave off this line of questioning. Regardless, these logical arguments seem to be not quite as convincing as including a plot which shows the laminated features remaining, even at a factor of 10 lower count rates. Figure 6 (now Figure 8) was an easy test to carry out, and the results are visually convincing. We have changed the beginning of this section to more clearly make the point in words within the Discussion section.

Change to manuscript:

The first paragraphs of this section now read:

"As discussed briefly in Section 3, the analyses are made using glued count rate profiles, which make use of photon counting signals in regions where the photon count rates are linear, and equivalent analogue signals in any region for which the photon counting rates become nonlinear. During routine processing, regions in which the analogue signals meet or exceed the counting limits of the analogue-to-digital converter are excluded from the retrieved profiles. For all measurements in this manuscript, the PMTs were not being operated near their maximum analogue count rates, so the likelihood of the laminations being PMT saturation artifacts is low.

Further, any saturation effects should serve to smooth out the profiles at high count rates, rather than inducing the oscillating count rates as we observe as the laminated cloud phenomena. In order to clearly demonstrate that these laminated features persist at much lower photon count rates, we performed a measurement with the aid of neutral density filters to lower the signal levels."

6b) Signal induced noise should be slow (microsecond time scale) and extensive in altitude.

Author response:

Agreed.

Change to manuscript:

We have removed the mention of signal-induced-noise in the first paragraph of section 5.1.

6c) PMT ringing on the other hand is something I would think could cause vertical structure on the scale described. I would think this is the major instrument effect to investigate.

Author response:

We agree that PMT ringing could, under the right circumstances which we do not believe to be the case here, produce repetitive vertical structure in lidar data on the scales described. However, (a) we would not expect to see PMT ringing if the PMT is not being saturated (covered in 6a, above - our PMT is not saturated), and (b) we would expect the effects to be different than what we see in the cloud measurements: In the case of classical PMT ringing, we expect a signal which starts at very high count rates, repeating higher-than-surrounding-values at regular altitude intervals, and amplitude damping out with height. In our case, the laminations look quite different to that description. Even in the event of some PMT ringing (which we do not believe to be present at all here), during which some residue of the ringing signature is combined with the geophysical results above, but it would be insufficient to explain all of the laminated features we see in our cloud measurements.

The new Section 5.2 has some specific explanations, including a comparison to a figure from Kovalev and Eichinger 2004.

Change to manuscript:

We have added a new subsection 5.2 to specifically address PMT ringing, entitled "Ruling out PMT ringing".

New reference:
[Kovalev and Eichinger 2004]
Kovalev, V. A. and Eichinger, W. E.: Elastic Lidar: Theory, Practice, and Analysis Methods, John Wiley Sons, Inc., Hoboken, New Jersey, 1 edn., http://gen.lib.rus.ec/book/index.php?md5=16F1687DEAF30CDD0E02BC46D0453F58, 2004. pp. 122 - 123, Figure 4.6

6d) I agree with your conclusion about laser power fluctuations. So much so that I would likely not even mention it in this analysis.

Author response:

We agree that it seems almost too obvious to mention, however this question has come up in every presentation of these plots to the atmospheric community. Upon short reflection, all of those asking the question could see that "of course!" laser power fluctuations cannot be causing the laminations, but it is one of the questions which has been ubiquitous in discussions. Further, an explicit statement that laser power fluctuations are not an issue for qualitatively detecting the laminations provides support for range-scaled photocount profiles being sufficient for the purposes of this manuscript (i.e. calibrated backscatter coefficient profiles are not requisite for the detection of the laminations). Therefore, the authors would prefer to mention it in the text if the referees can accept it remaining there.

6e) I agree mostly with your timing electronics conclusions but if you have an issue, it might not be stable in altitude. If you have 2 or more different clock speeds (from triggering, seeding, q switching, or your counting system clock drifting slightly), you could possibly alias one rate onto the other making your observations move in altitude. That would likely be a systematic shift observable at all altitudes though, and as such easy to identify.

Author response:

This is an interesting point which we had not previously considered. We'll keep it in mind for future analyses. The effects that we see do not seem to be systematic shift at all altitudes, so it is probably not the case here.

Referee Comment 7: I am surprised that the authors have not included lidar data that could be very helpful. They do call for more analysis in the conclusion. That said, without this analysis, I am not convinced that this work is a major observational contribution. Some omissions that I believe should be seriously considered (at minimum) are:

7a) I find myself surprised that the authors use radiosondes and not rotational Raman measured temperatures and vibrational Raman measured water vapor. This is especially true of Figure 4 where the thermodynamic structure changes dramatically over the observation period. The data need not be at 1 min resolution to be helpful.

Author response:

We would have loved to use both the Rotational Raman temperatures and Water Vapour measurements from CRL for this analysis for precisely the reasons pointed out by R1, however it was unfortunately not possible for this study. Major funding cuts to CRL's research program several years ago have prevented us from addressing the issues which came up with both Rotational Raman temperatures and Water Vapour:

Since the initial testing results of the Rotational Raman Temperature channels indicated in Nott 2012, we have found that the laboratory temperature cannot be sufficiently tightly controlled to produce reliable temperature measurements. The interference filters for the relevant channels must be controlled to within +/- 2 degrees C in order for the results to be meaningful, and this is something we cannot accomplish with our current setup. Thus we're unfortunately limited to non-lidar temperature profile results, and hence use radiosondes.

Similarly, our water vapour channel has not been continuously operational for the duration of the laminated cloud measurements. Additionally, the water vapour results from Rotational Raman techniques, as applied to CRL, are only fully valid in clear skies. As we are looking at clouds, and sometimes optically thick clouds, these results would not help as much as we might wish.

We will be interested to use results from other Eureka water vapour measurement instruments in the near future.

7b) I also find myself surprised that basic summary statistics of occurrence frequency or bounding relative humidity or temperature are not provided. At minimum, I would expect to see some observational bounds on conditions described in Section 5.4.

Author response:

Determining the statistics is outside the scope of this phenomenological study.

We intend to continue this project by exploring the frequency and distribution of such laminated clouds throughout the year. An intermediate step is to determine objective criteria by which we can determine whether a given time period of CRL data exhibits the required characteristics to be included vs. excluded from the population of laminated clouds. (How thin do the laminations have to be to qualify?

How many layers are required in a vertical sample? What amplitude in signal must these laminations have?). Likewise, we must determine a course to account for dates with no lidar measurements, and dates for which the lidar beam is attenuated at low altitudes - both being cases which do not preclude the existence of laminated clouds, but which would not be counted as a detection of them, either. These are not trivial tasks, so including a hard percent value for what percent of the time we see these clouds would be, at this stage, premature. Therefore in the current manuscript, we aim instead to simply point out that this laminated cloud phenomenon is not limited to wintertime measurements at Eureka.

We will make a comment regarding frequency at the start of Section 4: "Results".

Change to manuscript:

At the start of Section 4, insert the following text:

``**CRL made 182 days of measurements between March and December 2017. Of these, at least 45 days show evidence of horizontal laminations within clouds. Thus, laminations occurred on 25 % of all measurement dates. A minimum of one detection of laminations was present in each measured month. Hence, this phenomenon is not restricted to a particular season. March 2017 had highest rate of detections, with at least 10 of 24 measurement days demonstrating laminations. Three representative examples will be shown in full here: 21 March 2017 is in Section 4.1, 14 November 2017 is in Section 4.2, and 26 August 2017 is in Appendix C."**

7c) I am not sure raw photon counts are sufficient to quantitatively show the structures within clouds. Calibrated backscatter coefficients would be much more useful. Additionally, they remove uncertainty sources such as laser power fluctuations.

Author response:

Calibrated backscatter coefficient measurements require a normalization in clear air (or air of known aerosol backscatter cross-section for each measurement period. Typically, the region for this clear air is taken above any clouds and aerosol layers which are present. However, the clouds studied in this manuscript often nearly obscure any photons from heights above the clouds. At a minimum, the top parts of the clouds are likely to exhibit multiple scattering, and thus we cannot be sure of the returns above these levels. Likewise, a normalization region below the clouds is typically not available for these cloud examples, most of which extend down into our overlap region. Therefore the normalization for these dates is difficult.

Further, with CRL's SNR, we are unable to calculate calibrated backscatter coefficients at sufficiently high resolution to resolve these layers - this is presumably one reason that we had not noticed the laminations previously. The operational resolution for routinely retrieved CRL calibrated backscatter coefficients is 10 minutes x 105 metres.

Now that we have some motivation to examine the CRL data at high altitude resolution, we are investing further efforts into producing the best backscatter coefficient profiles we can.

We agree that raw photon counts are not ideal for a quantitative analysis of the amplitude of these laminations. However, given that no published works have, to our knowledge, done so much as to point out the existence of these laminations, we felt that publishing our findings that these laminations *exist at all* was important.

As pointed out by R1 in comment 7b, there are other quantitative results we can provide going forward, even with the raw counts profiles: Statistics about the occurrence rates for these features, and similar.

As also pointed out by R1 in comment 7d, laser fluctuations are not capable of producing false horizontal laminations in the plots. Given that this is the first paper to demonstrate the existence of these laminations in lidar data such as CRL's, we prefer to get the finding out into the community for further discussion as soon as possible (i.e. using range-scaled photocounts), and follow this up with calibrated backscatter profiles as becomes possible. There is lots of interesting quantitative follow-on work which should be pursued - and for that, we will surely address the effect of laser power from the measurements as much as we can.

Finally, the range-scaled photocounts presented here have been saturation/deadtime corrected, background corrected, PC and Analogue signals have been glued into a merged profile, and the plots are thus not quite raw profiles in any case.

Minor Comments:

Referee Minor Comment 1: Page 1, Line 4: It obviously depends on your target but 1 min time resolution might not be particularly high resolution. Suggest dropping the word “high” here. Also on Page 5, Line 10

Author response:

Done.

Our target is stable over a several minute period, so our measurements have high enough time resolution to detect these. We did want to make the point that observations at 20 minute time resolution, for example, are not as helpful - but it's true that lidars such as that in Hayman et al 2012 have much higher time resolution by a factor of over 100x.

Change to manuscript:

Removed the word "high" to make the sentence: **"CRL's time (1 min) and altitude (7.5 m) resolution ... "**

Referee Minor Comment 2: Figure 2: At 3km, the range correction should be 9X 10ˆ6. The counts that you are showing are therefore on the order of 10-100. Is that correct? If so, counting statistics worry me. It is impossible to tell here what wiggles are due to scattering phenomena and what wiggles are due to counting statistics. Suggest adding error bars to clarify.

Author response:

Yes, that range correction is correct, but the count rates are higher. The data are shown in MHz. The number of counts per measurement bin per unit time in this plot ranges from just under 600 photons/altitude bin/minute near 4 km, to over 10000 photons/altitude bin/minute at 3.15 km. The photon counting mode is used when raw signals are smaller than an equivalent to 20 MHz (N = 600 photons/bin/min) and the analogue mode is used above that. The uncertainties for the analogue mode include both poisson noise (approx. sqrt(N)) and systematic uncertainty introduced by the ADC

converter.

Here is the same data, shown in units of photocounts/bin/minute (not MHz), with shaded error bars, without altitude scaling, shown on a linear x-axis. The blue profile is located at its true position on the x-axis. The red, black, and green profiles are offset to the right of their true values by 5000, 10000, and 15000 photocounts respectively. The uncertainties are far smaller than the magnitude of the wiggles:

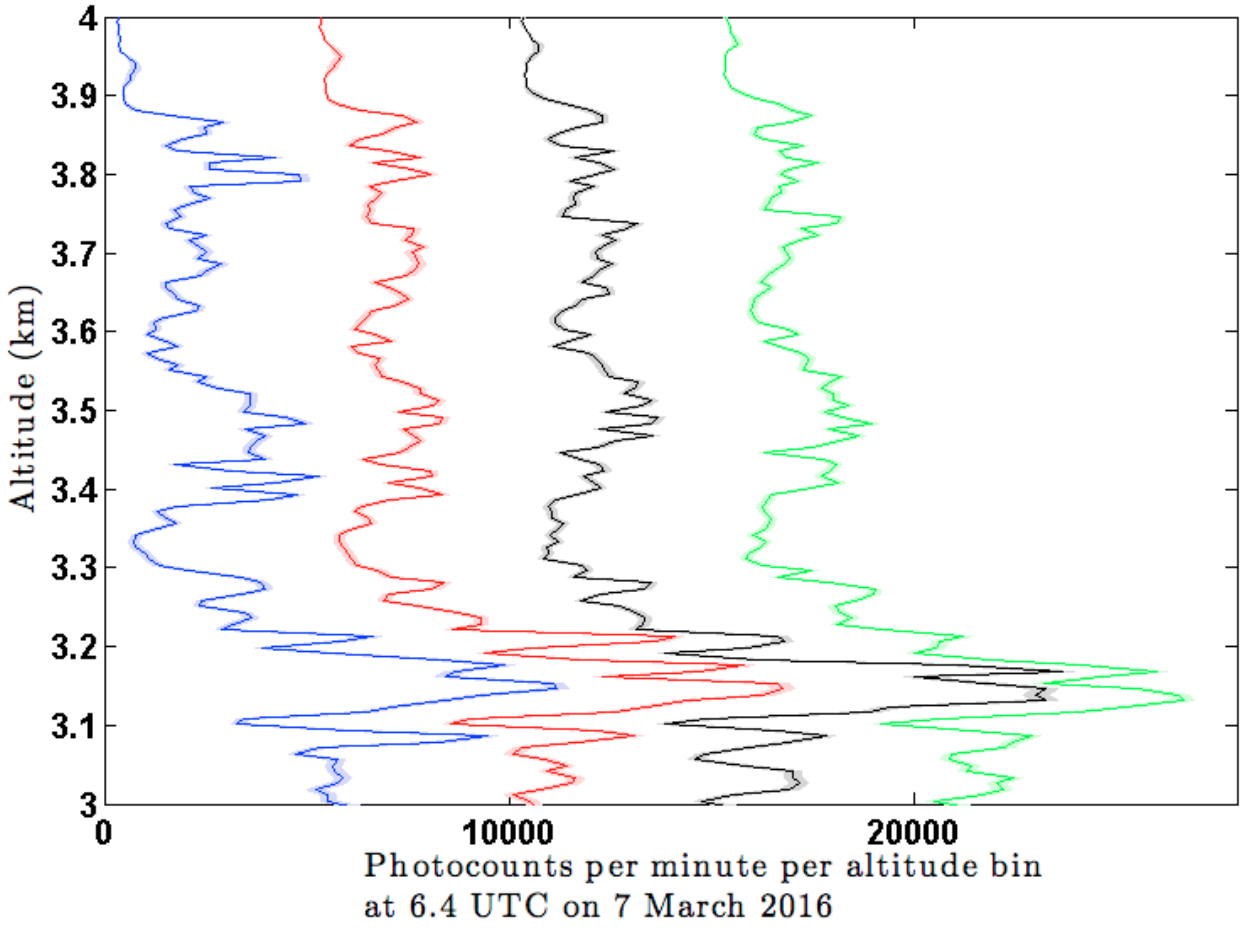

The wiggles due to counting statistics would be a larger worry if we had only one profile, and/or for channels which have fewer photons (e.g. depolarization perpendicular channel). However, statistical counting errors are likely to appear as white noise - as likely to be above as below the "true" profile. They should not be correlated in time for any given altitude. Given that we have profiles showing wiggles which *are* correlated in time, we consider that these are more likely to be due to scattering phenomena, and not counting statistics.

Change to manuscript:

We have added error bars to Figure 2 to indicate the extent of the uncertainty.

We have added the bolded text to the Figure 2 caption:

"Selected profiles of range-scaled 532 nm photocounts as a function of altitude for four consecutive

minutes just after 06:40 UTC on 7 March 2016 (same date as for Fig. 1), each offset by $1x10^{0.6}$ (or 4 m^2MHz) along the x-axis, between the altitudes of 3 to 4 km. **Shaded areas show uncertainty.** There are clearly horizontal coherent structures in the cloud in space (aliased to time by motion over the lidar) at least down to the 7.5 m height resolution of the lidar."

Referee Minor Comment 3: Page 3, Line 1-8: The following paper and references therein may be of interest to the authors as motivation for cloud structure size scales: Beals, et al., "Holographic measurements of inhomogeneous cloud mixing at the centimeter scale," Science 350, 87–90 (2015).

Author response:

Thank you for drawing our attention to this paper.

Changes to manuscript:

We have added a paragraph about this reference starting on Page 4 Line 3 (new version of manuscript). Following the paragraph which reads: "We have been unable to find many references to cloud features at sub-100m scales in the literature... Again, these situations are quite different in morphology from the laminated features described in this paper.", we add the new text:

"Measurements by airborne holographic imaging have visualized the spatial structure in clouds at centimetre scales by measuring droplet size and number distributions, revealing that clouds are inhomogeneous and contain sharp transitions between cloud and clear air properties even at the smallest turbulent scales (Beals et al. (2015)). Given that there are ``edges'' within clouds even at cm scales, it is reasonable to infer that there may be structural cloud features which are relevant to the overall interpretation of particular clouds, which are possible to investigate by lidar at resolutions of tens of metres and which will be missed entirely by lidar measurements at 100+ m scales. Certainly, the scales probed in Beals et al. (2015) are significantly smaller than those possible to investigate using the CRL lidar. Cloud measurements covering the entire range of spatial scales from centimetre to global is ultimately required. CRL helps close the gap from over four orders of magnitude of spatial size, to three, between the holographic imaging measurements and the smallest features currently discussed in the lidar literature."

We have also made reference to Beals2015 in the new Section 5.6 ``Suggested explanations for the laminated phenomena". See response to Reviewer 2, Comment #1, for the new text in that section.

New reference:
[Beals2015CloudHolography]
Beals, M. J., Fugal, J. P., Shaw, R. A., Lu, J., Spuler, S. M., and Stith, J. L.: Holographic measurements of inhomogeneous cloud mixing at the centimeter scale, Science, 350, 87 – 90, 2015.

Referee Minor Comment 4: Page 4, Line 17: Referring to a broad class of elastic scatter lidars as Mie lidars is very imprecise. Suggest modifying to "elastic scatter" as you have no way of verifying that all scatterers are spheres.

Author response:

The lidar which was deployed to Alert was explicitly called a "Mie Lidar" in Hoff 1998. The term "Mie

Lidar" in our sentence on Line 17 (old version) refers only to that particular lidar.

Referee Minor Comment 5: Page 6, Line 26: This sentence is confusing because your lidar counting system has already binned single photon data to 7.5 meters and 1 minute. Suggest modifying this sentence to something like: "No further binning was performed. "

Author response:

We have made this change.

Change to manuscript:

The sentence has been modified, as suggested by R1, to: "**No further binning was performed**".

Referee Minor Comment 6: Figures 3 and 4: I believe there are several ways to calculate relative humidity with respect to ice. There are several parameterized versions or more simple versions. They do not all result in identical values given identical inputs. Suggest adding a citation to describe the method you use.

Author response:

The Goff-Gratch formulation has been used for calculations.

Change to manuscript:

Appendix B has been added to the manuscript, which reads:

Appendix B: Calculations of RH over ice

Relative humidity with respect to liquid water (RHw) is converted to relative humidity with respect to ice (RHi) using the Goff-Gratch formulations for saturation vapour pressure (Goff and Gratch (1946), in List (1949)). Saturation vapour pressure over water, ew, can be calculated via equation B1:

$$\log_{10} e_w = -7.90298\left(\frac{T_s}{T}-1\right)+5.02808\log_{10}\left(\frac{T_s}{T}\right)-(1.3816\times10^{-7})(10^{11.344\left(1-\frac{T}{T_s}\right)}-1)$$
$$+(8.1328\times10^{-3})(10^{-3.49149\left(\frac{T_s}{T}-1\right)}-1)+\log_{10} e_{ws},$$

in which T is the radiosonde temperature in Kelvin, Ts = 373.16 K is the steam point temperature of liquid water, and ews = 1013.246 mb is the saturation pressure of liquid water at the steam point temperature (at 1 standard atmosphere). Saturation vapour pressure over ice, ei, can be calculated via equation B2:

$$\log_{10} e_i = -9.09718\left(\frac{T_o}{T}-1\right)-3.56654\log_{10}\left(\frac{T_o}{T}\right)+0.876793\left(1-\frac{T}{T_o}\right)+\log_{10}(e_{io}),$$

in which To = 273.16 K is the ice point temperature, and eio = 6.1071 mb is the saturation pressure of ice at the ice-point temperature (at 0.0060273 standard atmospheres). Relative humidity with respect to ice, in percent, is then equation B3:

$$RH_i = \left(\frac{e_w}{e_{io}}\right) RH_w$$

New references:

[GoffGratch1946LowPressureWater]
Goff, J. A. and Gratch, S.: Low-pressure properties of water from -160 to 212 F, in: Transactions of the American society of heating and ventilating engineers, pp 95-122, 52nd annual meeting of the American society of heating and ventilating engineers, New York, 1946.

[ListSmithsMetTables1949a6thEd]
List, R. J.: Smithsonian Meteorological Tables, vol. 114 of Smithsonian Miscellaneous Collections, Smithsonian Institution Press, 4th reprint (1968) of 6th revised edn., 1949.

Referee Minor Comment 7: Figure 4 Caption: Suggest shortening by describing panels a-f as "same as Figure 3" or similar.

Author response:

Done.

Change to manuscript:

We have revised the old Fig 4. caption (now numbered Fig. 6) text to read: **"Measurements from 14 November 2017; (a-f) same format as Fig. 4. Thick clouds were present early in the day, with cloud cover reducing later. Layers which start in a cloud continue in the next section of cloud, even if there is a gap in between. Precipitation alternated between light snow, blowing snow, ice crystals, and no precipitation at the ground throughout the day."**

Referee Minor Comment 8: Page 9, Lines 27-29: Low depolarization is consistent with observations of preferentially oriented ice crystals. Suggest clarifying that high depolarization is ": : :inconsistent with interpretation as randomly oriented ice particles." Note that the following might be of interest as well, especially Appendix A: Silber, et al., "Polar liquid cloud base detection algorithms for high spectral resolution or micropulse lidar data," J. Geophys. Res.: Atmos. (2018).

Author response:

We will clarify that low depolarization is inconsistent with randomly oriented ice particles, but is consistent with preferentially oriented ice particles.

Change to manuscript:

We have added text, as bolded here:
"The 45 m thick layers are displayed with a high depolarization parameter, which indicates non-spherical particles. Typically, this means **randomly oriented** frozen particles within clouds, or aerosol particles outside of clouds."

and
" The depolarization values in these regions are low and therefore combined with the high backscatter signal are consistent with liquid water droplets **and/or preferentially oriented ice particles**, and are inconsistent with interpretation as **randomly oriented** ice particles."

Referee Minor Comment 9: Page 10, Line 15 and elsewhere: I find the use of numbers like 1X10^10.5 to be difficult to interpret. Suggest changing to integer powers: 1X10^10.5=3X10^10 or much less preferably changing to dB.

Author response:

The non-integer powers are included for direct comparison to the log colour scale in the plots. We have now added in the brackets a conversion to integer powers after each instance in the text.

Change to manuscript:

For Fig. 2, the caption and corresponding text now reads: ... each offset by 1x10^0.6 **(or 4 m^2MHz**) ...

On Page 14, the brackets now read: (1×10^10.5 m2MHz rather than 1×10^10 m^2MHz**; equivalent to 3.2x10^10 m^2MHz vs. 1X10^10 m^2MHz**).

On Page 14, describing new Fig 6 (old fig 4): (1×10^8.8 **(or 6.2 x 10^8)**, red in Fig. 6b, and 1×10^8.5 **(or 3.2 x 10^8)** , yellow in Fig. 6c, respectively).

Referee Minor Comment 10: Page 11, Line 16-17 and throughout the manuscript: I assume your sondes are reporting their raw data with respect to water. Are you reporting all relative humidity values with respect to ice? It is clear in the figures but less so in the text. Suggest adding "w.r.t ice" or "w.r.t. water" throughout the text to clarify or inserting a blanket statement specifying how all data are reported.

Author response:

The sondes provide their raw data with respect to water. We then calculate the corresponding values with respect to ice where relevant (see response to R1 minor comment 6, above). We will clarify which RH is meant in each case in the text.

Change to manuscript:

Each instance of relative humidity in the text is now specified as with respect to water or with respect to ice in the manuscript.

Technical Corrections:

Referee Technical Comment 1: Page 10, Line 5: ": : :the air is remains: : :"

Author response:

Done.

Change to manuscript:

Correction made to: "... the air remains..."

Referee Technical Comment 2: Page 10, Line 14 and elsewhere: "The clouds[,] which contain: : :" The use of the word "which" requires use of a comma in most places.

Author response:

Here we intended no comma. We want to say that the [particular clouds which contain the layers] are found below 4 km, to clarify that not *all* CRL clouds are found below 4 km.

We have corrected this issue where it comes up in other locations.

Change to manuscript:

None at this location; commas added where needed elsewhere.

Referee Technical Comment 3: Page 19, Line 18: I believe the paper you refer to here is in the January 2012 publication, not 2011.

Author response:

We have made the correction. That article was published online 10 Dec 2011 and we had afterward neglected to update the reference to the final January 2012 publication date.

Change to manuscript:

Reference now reads: **Morrison, H., de Boer, G., Feingold, G., Harrington, J., Shupe, M. D., and Sulia, K.: Resilience of persistent Arctic mixed-phase clouds, Nature Geoscience, 5, 11–17, 2012.**

Lidar measurements of thin laminations within Arctic clouds

Emily M. McCullough[1,*], James R. Drummond[1], and Thomas J. Duck[1]

[1]Department of Physics and Atmospheric Science, Dalhousie University, 6310 Coburg Rd., PO Box 15000, Halifax, NS, B3H 4R2, Canada

Correspondence to: Emily McCullough (emccull2@uwo.ca)

Abstract.

Very thin (< 10 m) laminations within Arctic clouds have been observed in all seasons using the Canadian Network for the Detection of Atmospheric Change (CANDAC) Rayleigh-Mie-Raman lidar (CRL) at the Polar Environment Atmospheric Research Laboratory (PEARL; located at Eureka, Nunavut in the Canadian High Arctic). CRL's ~~high~~ time (1 min) and altitude (7.5 m) resolution from 500 m to 12+ km altitude make these measurements possible. We have observed a variety of thicknesses for individual laminations, with some at least as thin as the detection limit of the lidar (7.5 m). The clouds which contain the laminated features are typically found below 4 km, can last longer than 24 h, and occur most frequently during periods of snow and rain, often during very stable temperature inversion conditions. Results are presented for range-scaled photocounts at 532 nm and at 355 nm, ratios of 532/355 nm photocounts, and 532 nm linear depolarization parameter, with context provided by twice-daily Eureka radiosonde temperature and relative humidity profiles.

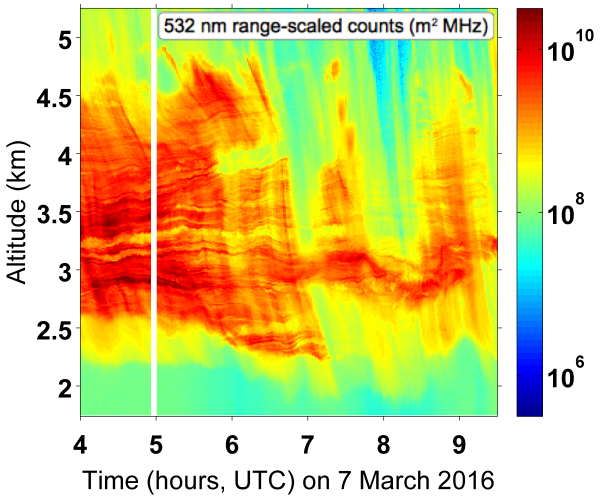

Figure 1. Thin laminated layers within an Arctic cloud. 532 nm range-scaled counts from the CRL lidar at Eureka, Nunavut showing quasi-horizontal layers, as thin as 7.5 m each, within a cloud on 7 March 2016, during snowing conditions.

1 Introduction

High resolution studies of clouds, and in particular Arctic clouds, are essential for a full understanding of the clouds' microphysical properties. Even if the clouds appear identical at low resolution, significantly different processes may occur in morphologically distinct clouds, e.g. a layered cloud in which the size of the layers is smaller than the resolution of the measuring instrument or model, and a smooth cloud with the same average optical properties as the layered cloud.

Figure 1 shows 532 nm range-scaled counts (counts $\times$ altitude^2) from the Canadian Network for the Detection of Atmospheric Change (CANDAC) Rayleigh-Mie-Raman lidar (CRL) at the Polar Environment Atmospheric Research Laboratory (PEARL; located at Eureka, Nunavut in the Canadian High Arctic). The figure shows quasi-horizontal layers, as thin as 7.5 m each, within a cloud on 7 March 2016, while snowing conditions were reported at the surface. CRL's highest resolution is required to resolve the thinnest laminations. There are descending features in Fig. 1 interpreted to be fall streaks. These do not seem to interfere with the persistence of the laminated features. There are at least 16 layers in the region between 3.25 and 3.75 km at 06:30 UTC, giving a mean layer thickness of 15 m. Some layers merge together into thicker layers, and split again into thinner layers, over the course of this 5.5 h plot. This example is not an isolated case. Similar phenomena are displayed frequently the CRL measurements, with individual cases often spanning several days in a row.

Figure 2 shows selected profiles of range-scaled 532 nm photocounts from Fig. 1 as a function of altitude for four consecutive minutes just after 06:40 UTC, each offset by $1x10^{0.6}$ (or 4 m^{2}MHz) along the x-axis, between the altitudes of 3 to 4 km. There are clearly horizontal coherent structures in the cloud in space (aliased to time by motion over the lidar) at least down to the 7.5 m height resolution of the lidar. The regions between the laminations generally exhibit range-scaled signals between 35 and 70 % lower than the signals of the laminations immediately above and below.

If the data are averaged to altitude bins 10 times as large as those shown, all traces of the laminated structure would be erased (Fig. 3), and the cloud would look ~~the same as~~ more similar to a smooth cloud. The higher resolution is required to have our interpretations approach a real representation of the cloud. Even in specific circumstances which could ensure that the layered cloud and the equivalent smooth cloud radiate equally overall, and thus influence the overall radiation budget in the same way, there is much to be learned about the disparate internal processes which form, maintain, evolve, and dissipate each of the clouds. Cloud-aerosol interactions, cloud condensation, particle growth, and precipitation are all microscale processes which may be better probed by measurements which can discern spatially inhomogenous cloud particle distributions from homogenous distributions. With a paucity of cloud measurements available in Arctic regions, as compared to mid-latitudes, high-resolution lidar measurements will be all the more valuable from polar laboratories.

High spatial and temporal resolution lidar measurements, particularly of cloud microphysical parameters, have been clearly stated in the literature as being desirable and necessary. The vertical size scales deemed to correspond to "high enough" spatial resolution, vary. Mioche et al. (2017), Loewe et al. (2017), and Hogan et al. (2003), make the case for sub-100 m sampling. Ramaswamy and Detwiler (1986), Korolev et al. (2007), Sotiropoulou et al. (2014) and Solomon et al. (2015) are several examples advocating for measurements at sub-50 m resolution. The current paper is concerned with measurements at sub-10 m scales.

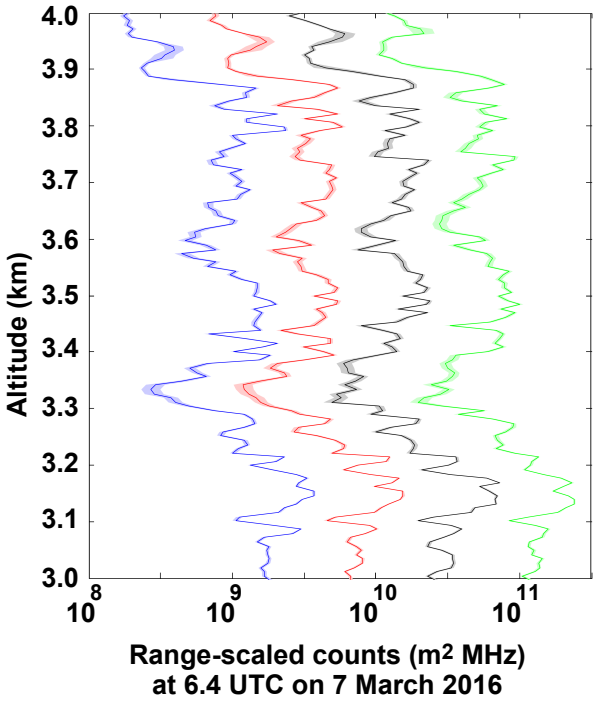

Figure 2. Selected profiles of range-scaled 532 nm photocounts as a function of altitude for four consecutive minutes just after 06:40 UTC on 7 March 2016 (same date as for Fig. 1), each offset by $1x10^{0.6}$ (or 4 m^2MHz) along the x-axis, between the altitudes of 3 to 4 km. Shaded areas show uncertainty. There are clearly horizontal coherent structures in the cloud in space (aliased to time by motion over the lidar) at least down to the 7.5 m height resolution of the lidar.

The literature, also, has many reports of vertically "narrow" or "very thin" measured features. These come at a large range of spatial sizes, generally larger than the scales that we are interested in here. Mid-latitude examples of "notably thin" features include: Sassen et al. (2005), who describe a "remarkably narrow" feature (a dark-(lidar) and bright-(radar) band attributed to regions of snowflake melting) with a full width half maximum (FWHM), estimated from their Fig. 4, of approximately 500 m. Since a resolution of 75 m was used, higher resolution features should have been detectable had there been any present. Hayman et al. (2012) used a higher resolution lidar (7.5 m x 0.5 s) in Boulder, Colorado, USA to detect a "narrow altitude band" of differently oriented scatterers which extends between 5 and 5.5 km, and therefore is 500 m in vertical extent. Hogan et al. (2003) ran aircraft measurements over the UK, with some analysis possible at 15 m resolution, and they describe "thin layers of high [attenuated backscatter coefficient] around 150 m thick", and others 100 m to 200 m thick.

We have been unable to find many references to cloud features at sub-100 m scales in the literature. Indeed, it is difficult to find any reference to multiple layers within clouds (as in Fig. 1) as opposed to multiple layers of clouds (2 or 3 separate clouds at different altitudes, separated by hundreds of metres to several kilometres, e.g. Curry et al. (1988)). Likewise, thin (100 - 200 m thick) layers of supercooled liquid water are known to frequently top mixed-phase clouds, generally precipitating ice

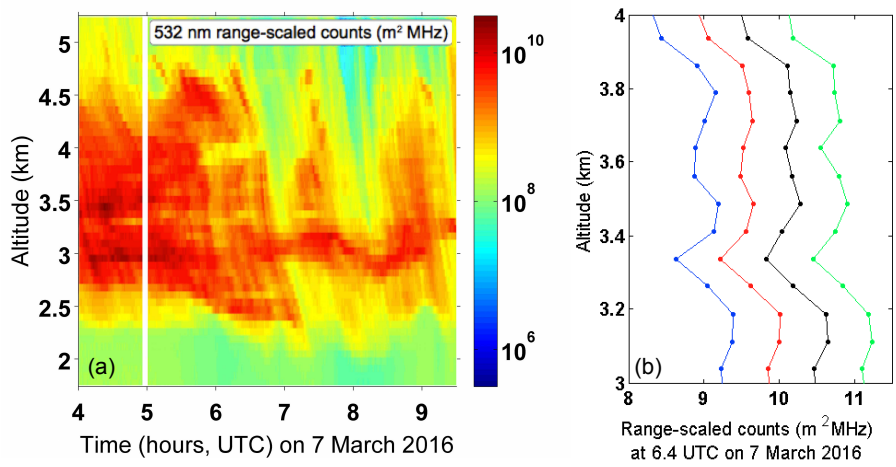

Figure 3. Same measurements as Figs. 1 (a) and 2 (b), recalculated with altitude bins 10 times as large. Resolution is 1 min X 75 m. The fine (< 10 m) laminations are no longer discernible. Only the much larger features (e.g. between 3.2 and 3.4 km) remain.

~~(Morrison et al., 2011; Shupe et al., 2008)~~(Morrison et al., 2012; Shupe et al., 2008). Again, these situations are quite different in morphology from the laminated features described in this paper.

Measurements by airborne holographic imaging have visualized the spatial structure in clouds at centimetre scales by measuring droplet size and number distributions, revealing that clouds are inhomogeneous and contain sharp transitions between cloud and clear air properties even at the smallest turbulent scales (Beals et al. (2015)). Given that there are "edges" within clouds even at cm scales, it is reasonable to infer that there may be structural cloud features which are relevant to the overall interpretation of particular clouds, which are possible to investigate by lidar at resolutions of tens of metres and which will be missed entirely by lidar measurements at 100+ m scales. Certainly, the scales probed in Beals et al. (2015) are significantly smaller than those possible to investigate using the CRL lidar. Cloud measurements covering the entire range of spatial scales from centimetre to global is ultimately required. CRL helps close the gap from over four orders of magnitude of spatial size, to three, between the holographic imaging measurements and the smallest features currently discussed in the lidar literature.

The closest description that we have found to the laminations, and which indeed may show the identical phenomenon, comes from Hobbs and Rangno (2008), with cloud particle concentration and size measurements from airborne campaigns over the Beaufort Sea in April 1992 and June 1995. Their vertical profiles of cloud droplet concentrations show "adjacent layers, separated by only tens of metres ... often exhibiting substantially different droplet concentrations". They infer that the layers are not mixing with one another, and note that more non-mixed clouds are observed than mixed ones during the campaigns. Their Fig. 4 is demonstrates these layers. Like CRL's results, the horizontal flight path of the aircraft aliases spatial and temporal phenomena somewhat: "In some cases cloud layers separated by short distances merged together for a time", as indicated by the aircraft flying into a sudden region of increased liquid water content. CRL sees something similar, with

individual layers seeming to merge and separate along the time axis of the photocount plots. Hobbs and Rangno (2008) note multiple temperature lapse rates within single clouds, usually including regions of stability. Slight stability is noted as a cause for non-mixing in some cases, but is not present in all non-mixed (multiple-layered) cases. This leaves open some room for investigation into the mechanisms of formation and persistence of the layers.

If we extend our search to include studies of Arctic haze, more numerous results are available at high vertical resolution, and references are made to thin layers within a particular single unit of haze. There was a Mie lidar present at Alert, Nunavut, Canada for 9 weeks in 1984-5 (Hoff, 1988) for the purpose of studying the vertical distribution of Arctic haze. Its 694.3 nm laser with 4.6 m maximum vertical resolution measured layers as thin as 100 m in several cases, but none of these had the laminated morphology seen by CRL. Several aircraft campaigns have shown stacked haze layers on the order of tens of metres thick. Radke et al. (1989) used a 1064 nm downward-pointing aircraft lidar with resolution 3 m vertically x 40 m horizontally. It flew for two days in March 1986, ending in a polar airmass over Baffin Island which contained thin layers of haze. They are described as "multiple thin, discrete laminae. Some of the hazes observed by us in the Arctic have been < 20 m thick". These features approach the same order of magnitude as the cloud features observed by CRL which are presented in the present paper. Brock et al. (1990) made a flight one month later in April 1986 between Thule, Greenland, and Søndre Strømfjord, Greenland. The results include multiple thin haze layers of thickness between 30 and 60 m, separated by regions of similar thickness of cleaner air. These campaign results were confirmed a decade later by Khattatov et al. (1997), who ran an extended aircraft campaign and again found highly stratified haze over not only the Canadian Arctic, but over Russia and Germany as well. Figure 2 of Morley et al. (1990), which measured using 3 m and 7 m resolution modes, provides a plot which is strikingly similar to many shown later in the current paper. The differences are that while Morley et al. (1990) shows laminated aerosol layers 200 to 300 m thick, the CRL measurements are of laminated cloud layers which are closer to 10 m thick, and which are thus an order of magnitude smaller. All of the laminated haze layer reports are from aircraft campaigns of short duration, and all excluded from consideration any measurements which included ice crystals and clouds.

In mid-latitude examples of extremely strong atmospheric boundary layer stability, striations of fog may be identified at scales smaller than 1-metre (Mahrt (2014), Fig. 3). These are qualitatively similar to the cloud laminations identified by CRL. Perhaps the two phenomena share similar properties, particularly in terms of the factors which enable the laminations/striations to persist.

There is room for further investigation of clouds by lidar at size scales of tens of metres and smaller. The measurements presented in this paper begin to fill this gap in our measurement record, and demonstrate that finely laminated cloud features are present in Arctic clouds in the Canadian Arctic at all times of year. The laminated haze layers described in the literature are qualitatively similar in appearance to, and thus may share similar origins or mechanisms of persistence with, the laminated cloud layers presented here from CRL.

2 The CRL Lidar at Eureka, Nunavut

The Canadian Network for the Detection of Atmospheric Change (CANDAC) Rayleigh-Mie-Raman lidar (CRL) makes observations at the Polar Environment Atmospheric Research Laboratory (PEARL) at Eureka, Nunavut in the Canadian High Arctic (80° N, 86° W).

CRL makes measurements at high resolution in altitude (7.5 m) and time (1 min) from 3.75 m to 120 km altitude. Above about 60 km, the lidar receives photons only from the sky background (scattered sunlight, moonlight, etc). Most of the signal from laser photons which are scattered by cloud and aerosol particles return from altitudes less than about 30 km. With analyses carried out CRL's highest resolution, retrievals are available from 500 m to 12+ km altitude. With overlap corrections, retrievals below 500 m are possible (Rotermund et al., 2014). Using coadding of signals (i.e. lower spatial or temporal resolution), retrievals to higher altitudes (e.g. 20+ km) are routinely available (e.g. Zhao et al. (2014) and Lindenmaier et al. (2012)). See Nott et al. (2012) for a description of CRL and McCullough et al. (2017) for an updated description of its depolarization system. The relevant measurement channels for the present paper are the 355 nm Rayleigh elastic channel, the 532 nm Raleigh elastic channel, and the 532 nm depolarization channel.

3 Data reduction

Low-level data corrections as in McCullough (2015) and McCullough et al. (2017) have been applied to all raw photocount measurements. Namely, all photon counting data have been dead-time corrected and background subtracted; all analogue data have been dark count profile corrected, have been mapped from unitless measured values to the corresponding photomultiplier (PMT) voltages based on hardware settings, have been background subtracted, and have been converted from units of mV to equivalent photon count rates using gluing coefficients found during calibrations; the photon counting and analogue signals have been merged together to create a single profile of photon count rate over all available signal levels for each channel. This value is expressed in MHz, which indicates the measured signal rate for each altitude bin, for each profile.

Typically, CRL data would be binned by co-adding in either altitude or time. This increases the signal to noise ratio (SNR) of the measurement, at the cost of reducing its resolution. For all plots in this paper, no post-integration of lidar photon counts was performed. We keep maximum resolution, at the cost of having some somewhat noisier plots at the higher altitudes. This enables us to locate features with sizes on the order of one altitude bin (provided they last some time), or one time bin (provided there is some extent in altitude) for further study.

The 532 nm and 355 nm measured signal rates are multiplied by the square of the altitude of each data point to remove geometric altitude bias from the plots. The resulting range-scaled photocounts are then plotted on a logarithmic scale. Examples of such plots are given in Fig. 1, and in panels a, b, and c of Figs. 4 and 6. The range-scaled photocount plots have not been normalized for laser power fluctuations, which are expected to remain $\leq 5\%$. Therefore, we can trust relative signal variations within each vertical profile of a plot more strongly than we can trust relative signal variations in time. One notable exception is the region below about 750 m altitude which is the region of incomplete geometric overlap for CRL. No overlap corrections have been made, so signals below this altitude may not be properly normalized with respect to the rest of the profile.

The second type of plot presented in this paper is a ratio of 532 nm to 355 nm measured signal rates. This is not the traditional 'colour ratio' sometimes published in lidar literature, since it is directly the ratio of signal rates, and is not a ratio of calibrated backscatter coefficient values. Examples of these plots are Figs. 4d and 6d.

The third type of plot in this paper is 532 nm linear depolarization parameter, calculated as per the d_1 method from McCullough et al. (2018): $d = (2kS_\perp)/(S_\parallel + kS_\perp)$. $S_\perp$ is the signal measured by the perpendicular channel, $S_\parallel$ is the signal measured by the parallel channel, and k is the depolarization calibration constant ($k = 21$ for CRL). The depolarization may also be expressed as the depolarization ratio, which can be calculated directly from depolarization parameter: $\delta = d/(2-d)$. At CRL, the parallel and perpendicular channels share a single PMT. A Polarotor rotating prism with timing electronics admits received photons to each measurement profile on alternate laser shots. Examples of depolarization parameter plots are Figs. 4e and 6e. Appendix A provides some plots of depolarization uncertainty in Figs. 9 and 10.

Temperature and humidity profiles obtained using radiosondes launched from the Eureka Weather Station are also provided. No additional corrections have been made before plotting. The relative humidity values are plotted ~~as the more relevant relative humidity over ice for the winter examples, and over water for the summer example~~with respect to both water and ice in all cases. Examples of these plots are Figs. ~~4f,g and 6f,g~~5c,d and 7c,d.

4 Results

CRL made 182 days of measurements between March and December 2017. Of these, at least 45 days show evidence of horizontal laminations within clouds. Thus, laminations occurred on 25 % of all measurement dates. A minimum of one detection of laminations was present in each measured month. Hence, this phenomenon is not restricted to a particular season. March 2017 had highest rate of detections, with at least 10 of 24 measurement days demonstrating laminations. Three representative examples will be shown in full here: 21 March 2017 is in Section 4.1, 14 November 2017 is in Section 4.2, and 26 August 2017 is in Appendix C.

4.1 Layers present for 24 hours on 21 March 2017

On 21 March 2017, the 532 nm range-scaled counts show thin layers persisting through a 2 km thick cloud which is present for about 21 h as shown in Fig. 4a. The clouds began on the previous day (08:15 UTC 20 March 2017), and continued for another 2 h on the following day (until 02:00 UTC 22 March 2017). The portion of Fig. 4a inside Box A has been reproduced in a larger format for Figs. 4b,c,d,e, to show detail. Resolution for all colour plots is 1 min x 7.5 m. ~~The lidar data was not binned~~No further binning was performed.

Figure 4b is 532 nm range-scaled counts, and we can discern layers of several thicknesses within this area. The layers are quasi-horizontal, but can move vertically by small amounts (usually less than 50 m) over hours-long timescales. Below 1 km at 22:00 UTC there are some layers approximately 45 m thick each. At 1.25 km at 23:00 UTC, there are layers 22.5 m thick interspersed with the thicker layers. A grouping of 4 layers is particularly noticeable at 2 km at 22:30 - 24:00 UTC, each layer having a thickness of 15 to 22.5 m. Many other thin layers are also present within this plot. Similar plots were examined at 2

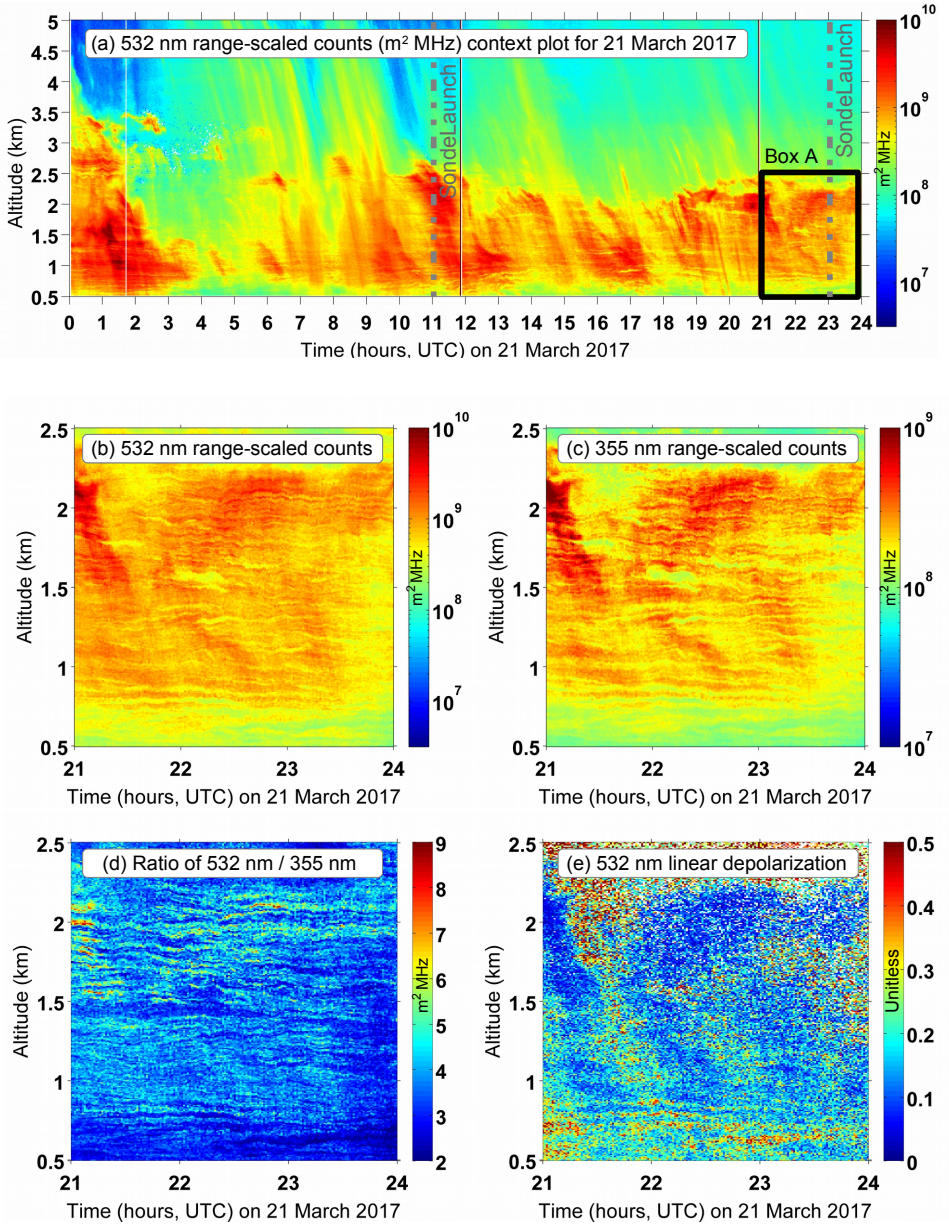

Figure 4. Measurements from 21 March 2017. Clouds persisted for the majority of the day, with thin layers visible in all clouds below 3 km altitude. Fall streaks indicative of precipitating particles are frequently present. This instance of laminated cloud lasted in excess of 42 hours, beginning on the previous day, and ending on the following day. **(a)** is a context plot of 532 nm range scaled photocounts. **(b, c, d, e)** are detailed plots for the region indicated by the black Box A of **(a)**. **(b, c)** are 532 nm and 355 nm range scaled photocounts, respectively; **(e)** is the ratio of 532/355 nm photocounts; **(e)** is the 532 nm linear depolarization parameter.~~**(f, g)** give the temperature and relative humidity with respect to ice from the two daily rasiosondes launched by the Eureka Weather Station. Grey solid lines in **(f)** are dry adiabats, and grey dashed lines are moist adiabats.~~

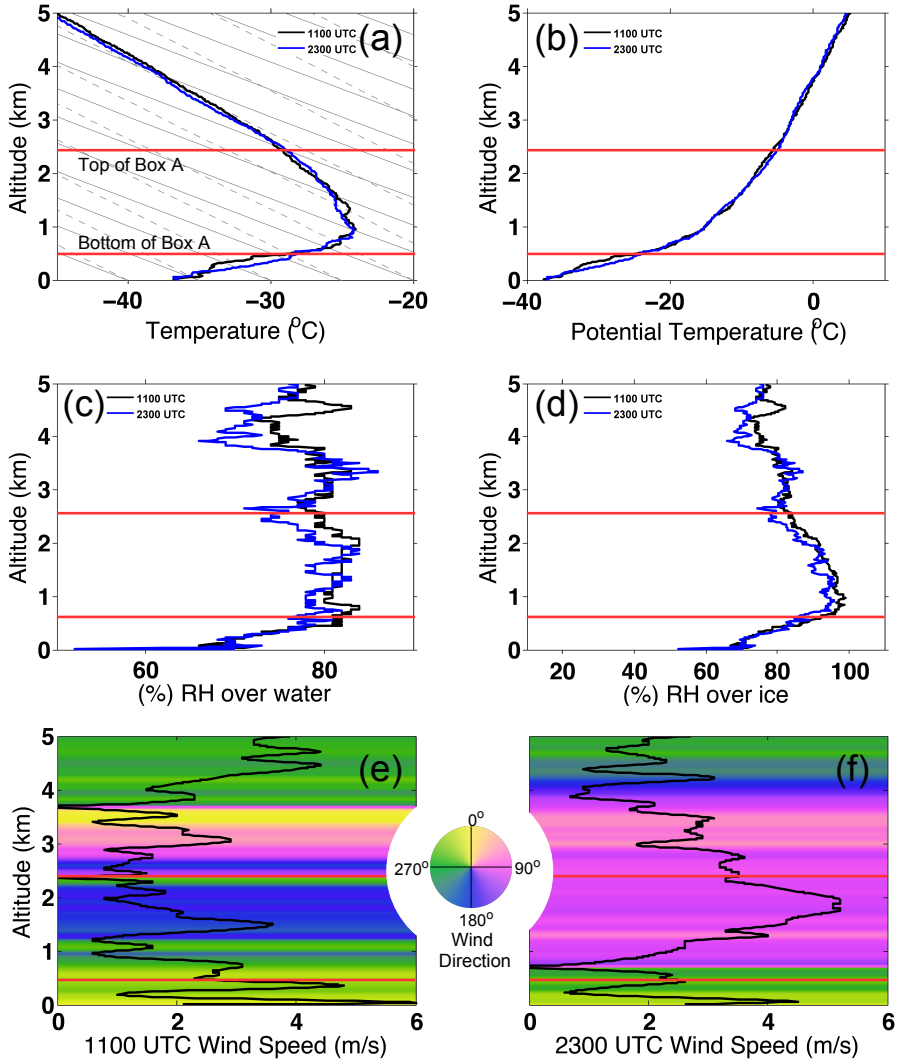

Figure 5. 21 March 2017. From the two daily rasiosondes launched by the Eureka Weather Station: **(a)** is the temperature; grey solid lines are dry adiabats, and grey dashed lines are moist adiabats. **(b)** is the potential temperature. **(c,d)** are the relative humidity with respect to water and ice respectively. **(e,f)** are the wind speed (black line) and direction (coloured background). Red lines show top and bottom altitudes of Box A from Fig. 4.

x 2 data binning (to a resolution of 2 min x 15 m; not shown). As expected, all layers thicker than 7.5 m were still visible, but their edges were less well-defined. The 7.5 m thick layers were sometimes still visible, and sometimes not, with longer-lasting layers being easier to see. Several instances of fall streaks are visible within the plot, apparent from their descent in time. The fall streaks do not seem to prevent the continuation of the laminations within the cloud.

Figure 4c is 355 nm range-scaled counts. All bright layers visible in the 532 nm plot are also visible as enhancements in the 355 nm plot. The 355 nm channel has lower overall photon count rates than the 532 nm channel, so some of the weaker layers in terms of backscattered photon amplitude are not picked up in the 355 nm plot. For example, there is a pair of 7.5 m thick layers at 1.8 km just after 02:00 UTC which are seen in the 532 nm plot, but not in the 355 nm plot. All layers to which the 355 nm plot is sensitive are present also in the 532 nm plot.

Fig. 4d is the ratio of the 532 nm/355 nm MHz count rates. We see many of the same thin layered features in this type of plot. The thicker 45 m layers are clearly seen, as well as most of the brighter layers above 1.5 km which are thicker than 22.5 m. Layers as thin as 7.5 m which were identified in the individual plots for 532 nm and 355 nm can be found in this ratio plot, but they are not so obvious. This is not a traditional colour ratio, since it is taken between the count values themselves, and not between backscatter coefficient values. Nevertheless, the presence or absence of layers in the ratio plot, which are present in the individual plots, can provide extra information about the geophysical phenomena which form the layers. For certain particle size distributions, we may expect not to see the layers in such a calculation, despite their presence in the atmosphere. A more sophisticated approach to a colour ratio has been used to combine CRL measurements with radar measurements in Bourdages et al. (2009), but the resolution of the available radars at Eureka is not sufficient to resolve the 7.5 m features we see here.

Figure 4e is the 532 nm linear depolarization parameter. This is calculated using the d_1 method from McCullough et al. (2018), which is the technically simplest method to calculate the desired quantity. The downside of the method is that one of the measurement channels has very low signal rates, leading to a generally low signal to noise ratio (SNR). Consequently, the depolarization plot shown here is noisy, and the layers are difficult to discern. The 45 m thick layers are displayed with a high depolarization parameter, which indicates non-spherical particles. Typically, this means randomly oriented frozen particles within clouds, or aerosol particles outside of clouds. There are some small features which have higher depolarziation parameters than the surrounding areas, but which do not correlate with the layers seen in 4a,b,c. For example, the $d_1 = 0.25$ feature just below 1.5 km altitude which rises slightly between 21:00 and 21:30 UTC, and the parallel line about 0.2 km below it. The regions between the layers of high 532 nm backscatter, therefore, are the regions consistent with an interpretation of ice or aerosol particles. The regions within the high backscatter layers are not. The largest blue swathes in the depolarization plot correspond to general regions of the highest photocount rates in the 532 nm plot. The depolarization values in these regions are low ~~,~~ and therefore combined with the high backscatter signal are consistent with liquid water droplets and/or preferentially oriented ice particles, and are inconsistent with interpretation as randomly oriented ice particles.

~~Figures 4f and g~~ Although the depolarization plots are somewhat noisy at this resolution, absolute uncertainties are generally between 0.05 and 0.1 (in the same units as depolarization parameter) for the region below 1 km, where the laminations are visible in Fig. 4e. At higher altitudes, uncertainties for this date reach 0.16.

Figures 5a and b display measurements of temperature and ~~percent relative humidity~~potential temperature, respectively, from ~~a~~ Eureka Weather Station radiosonde flights which took place at 11:00 and 23:00 UTC. The sonde data is plotted ~~on the same altitude scale as~~ from 0 to 5 km to provide context for the plots in Fig. 4~~a, and the 23:00 UTC flight falls within the time range of plots b,c,d,e~~. The red lines on ~~plots f and g~~ all Fig. 5 plots indicate the upper and lower altitude bounds of Box A from Fig. 4a, which are also the altitude bounds of Figs. 4b,c,d,e. The 23:00 UTC flight falls within the time range of Figs. 4 b,c,d,e. Dry and saturated adiabats, in solid and dashed grey, respectively, provide a guide to the thermal stability within the cloud.

Figure ~~4f~~ 5a shows a strong temperature inversion whose temperature starts at -36° C at the ground, increasing to -28° C by the bottom edge of Figs. 4b,c,d,e, to a maximum temperature of -24° C at 1 km altitude, before the temperature starts decreasing throughout the troposphere. By the top edge of Figs. 4b,c,d,e the temperature has decreased to -29° C, and by the top edge of Figs. 4a at 5 km altitude, the temperature is -46° C. Some background information regarding temperature inversions for the Arctic is available in Lesins et al. (2012). Even above the temperature inversion thermal maximum, the air ~~is~~ remains very stable, as indicated by comparison with the adiabatic lapse rates.

~~Figure 4f gives the relative humidity with respect to ice to be between 85 % and 97 % through~~ The temperature profiles for both sondes are quite similar in shape. Figure 5b shows potential temperature for both sondes smoothly increasing from the ground to 1 km at a rate of about 22.2° C/km, and at a larger rate of 5.0° C/km at higher altitudes.

Figures 5c and d give the relative humidity over water and over ice (See Appendix B), respectively, for both sondes. Through the regions of 4b,c,d,e, ~~varying between about 70~~ relative humidity over water varies between 75 % and ~~98~~ 85 %~~through~~, while relative humidity over ice varies between 85 % and 97 %. Through the full region plotted in ~~4a.~~ Fig. 4a, relative humidity over water remains between 65 % and 85 %, and relative humidity over ice remains between 85 % and 97 %. In both cases, the relative humidity increases very quickly from the ground up to 750 m altitude, before levelling off for relative humidity over water, and ultimately decreasing for relative humidity over ice. The relative humidity plots are relatively constant from sonde to sonde on this day.

Hourly metorological observations recorded by the Eureka Weather Station on 21 March 2017 note precipitation at ground level throughout the day: ice crystals at 00:00 UTC and 01:00 UTC, snow at 02:00 UTC through 12:00 UTC, and ice crystals again thereafter. The temperature recorded at the weather station varied between -35.7° C and -37.9° C during this time.

To explore the dynamics, Figure 5 shows wind speed (line plot) and direction (coloured background) in panels e and f from the 11:00 UTC and 23:00 UTC sondes. The wind profiles differ considerably in direction between the two sondes, although the magnitude of the windspeeds are of the same order of magnitude: between 0 and 5 m/s. The wind direction is much more variable in height for the 11:00 UTC sonde. Below 1.25 km, the wind is generally around 280°, at which point it rotates to about 180° until 2.5 km, then to 90° until 3.5 km, before returning by 4 km to a direction of 270°. Throughout the profile, there are small altitude ranges (e.g. at 2.3 km) which show larger windshear, but generally the change in wind direction is relatively gradual, with few complete reversals of direction. The 23:00 UTC profile, conversely, begins with wind direction at the same 280° direction from the ground to 750 m, then reverses to about 100° and remains constantly from this direction until 4 km, at which point it returns again to 260°. There are no instances of quick oscillations of wind direction with altitude in the 23:00 UTC profile which would be similar to those in the 11:00 UTC profile. In the region of Figs. 4b,c,d,e, the 23:00 UTC

wind profiles are relevant from 0.5 to 2.5 km, a region which includes one reversal in wind direction just below 1 km altitude. At this location, the wind speed reaches zero as it changes from a generally decreasing profile in one direction to a generally increasing profile in the opposite direction. Around 2 km, the windspeed reaches a maximum of 5 m/s and then decreases.

4.2 Layers reappearing several times on 14 November 2017

On 14 November 2017, the 532 nm range-scaled counts in Fig. 6 show thin layers similar to those in the 21 March 2017 example (Fig. 4). The clouds which contain the layers are slightly different. The day begins with clouds thicker in vertical extent (4.5 km rather than 3.5 km), with peak count rates 3 times larger ($1\times10^{10.5}$ m^{2}MHz rather than 1×10^{10} m^{2}MHz; equivalent to 3.2×10^{10} m^{2}MHz vs. 1×10^{10} m^{2}MHz). There is some internal layering during the cloud from 01:00 to 08:00 UTC with layers on the order of 7.5 m up to 50 m thick. This thick cloud lasts until about 08:00 UTC, at which point it diminishes drastically in optical thickness, and then becomes discontinuous for the rest of the day. The thinner, patchy clouds after 12:00 UTC are restricted to altitudes below 2.5 km.

Layers which start in a cloud continue in the next section of cloud, even if there is some non-cloudy region in between. The layers seem contiguous. The layers seem to continue between periods of fall streaks indicative of precipitating particles. Around 11:00 UTC at 1.3 km, 1.6 km, and two layers near 2 km, we can see some remnants of these layers with photocount values that would seem to indicate aerosols, and not cloud particles, between the obvious clouds. This is more apparent in the 532 nm and 355 nm range scaled counts plots when the colourbar is rescaled (not shown), and can be seen in the colour scale for the ratio 532/355 nm plot in Fig. 6c.

The plots of 14 November 2017 are a good example of a day which has both layered clouds (01:00 - 11:30 UTC; 22:30 - 23:30 UTC) and clouds without layers (12:00 - 21:00 UTC).

Some of the layers are visible in the depolarization parameter plot, Fig. 6d, but not all of them. This is likely to be a sensitivity issue in some regions, as we are operating at the detection limit of the depolarization's perpendicular measurement channel. In other regions, such as in the prominent fall streak visible as bright green at the bottom left corner of the plot, extending from 01:30 km at 09:30 UTC to 0.5 km before 10:00 UTC, sensitivity is unlikely to be the reason that the layers are not visible. There, since backscatter is high, and depolarization $d = 0.5$ is high also, precipitating frozen particles are a reasonable interpretation. We do not see any layering in this type of feature in any of the plots. For the regions in which we do see laminated depolarization, the depolarization parameter is anticorellated with photon count rate at both wavelengths in Fig. 6. The depolarization parameter is low (values of less than 0.1, dark blue in Fig. 6e) when the count rates in both the 532 and 355 nm channels are high ($1\times10^{8.8}$ (or 6.2×10^{8}), red in Fig. 6b, and $1\times10^{8.5}$ (or 3.2×10^{8}), yellow in Fig. 6c, respectively). One particular layer which demonstrates this quite clearly is at 0.6 km altitude, from 10:30 UTC - 10:45 UTC. This layer is dark blue (low values) in the depolarization parameter plot, but red and yellow (high values) in the 532 nm and 355 nm range scaled counts plots. Corresponding 532/355 nm values are also high. Therefore, as for the 21 March 2017 example, we interpret the laminations with high backscatter and low depolarization to be most likely liquid particles, and unlikely to be aerosol or ice. Conversely, the spaces between the high backscatter laminations exhibits higher depolarization which, combined with low backscatter values, leads to a reasonable interpretation of aerosol particles.

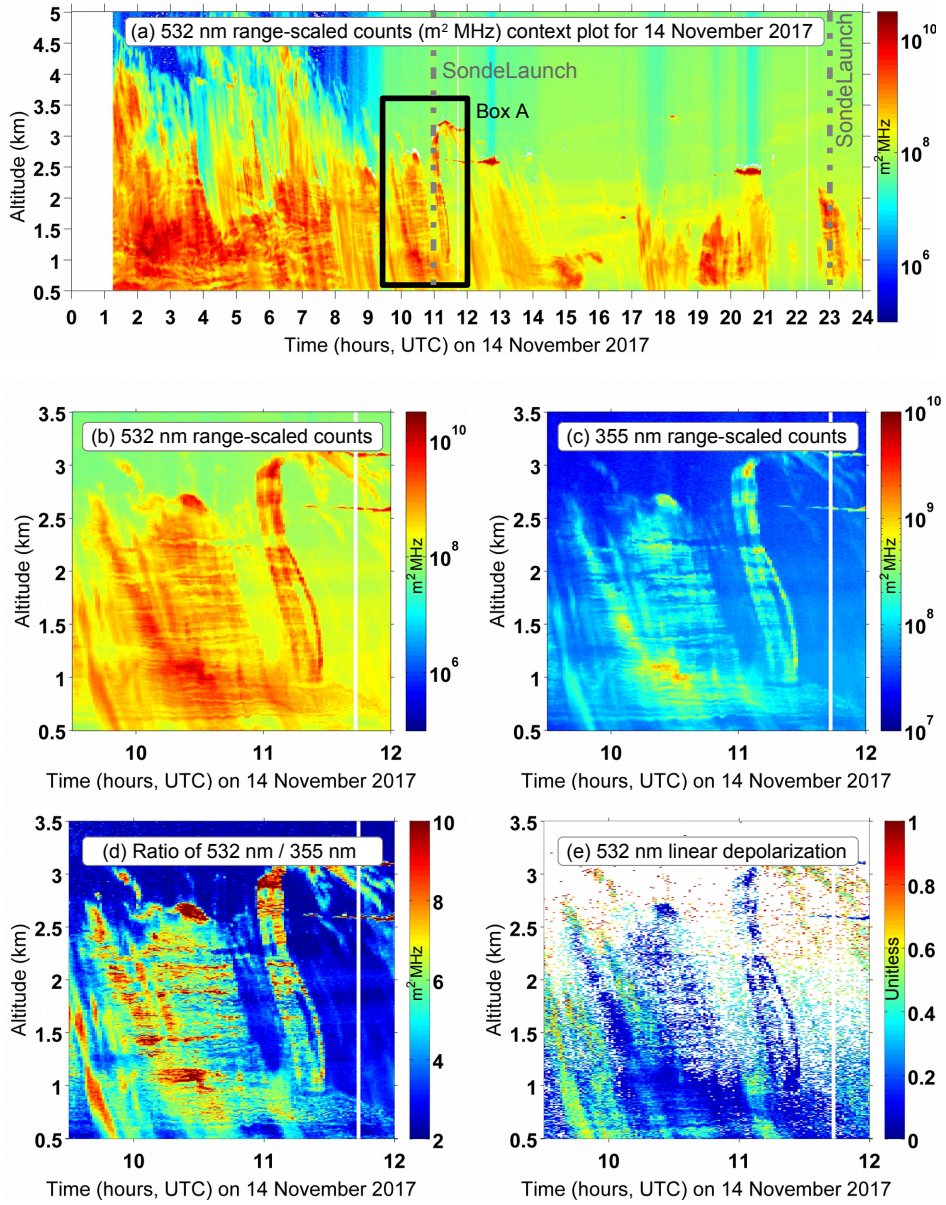

Figure 6. Measurements from 14 November 2017; **(a-e)** same format as Fig. 4. Thick clouds were present early in the day, with cloud cover reducing later. Layers which start in a cloud continue in the next section of cloud, even if there is a gap in between. Precipitation alternated between light snow, blowing snow, ice crystals, and no precipitation at the ground throughout the day. ~~**(a)** is a context plot of 532 nm range scaled photocounts. **(b, c, d, e)** are detailed plots for the region indicated by the black Box A of **(a)**. **(b, c)** are 532 nm and 355 nm range scaled photocounts, respectively; **(c)** is the ratio of 532/355 nm photocounts; **(e)** is the 532 nm linear depolarization parameter. **(f, g)** give the temperature and relative humidity with respect to ice from the two daily rasiosondes launched by the Eureka Weather Station. Grey solid lines in **(f)** are dry adiabats, and grey dashed lines are moist adiabats.~~

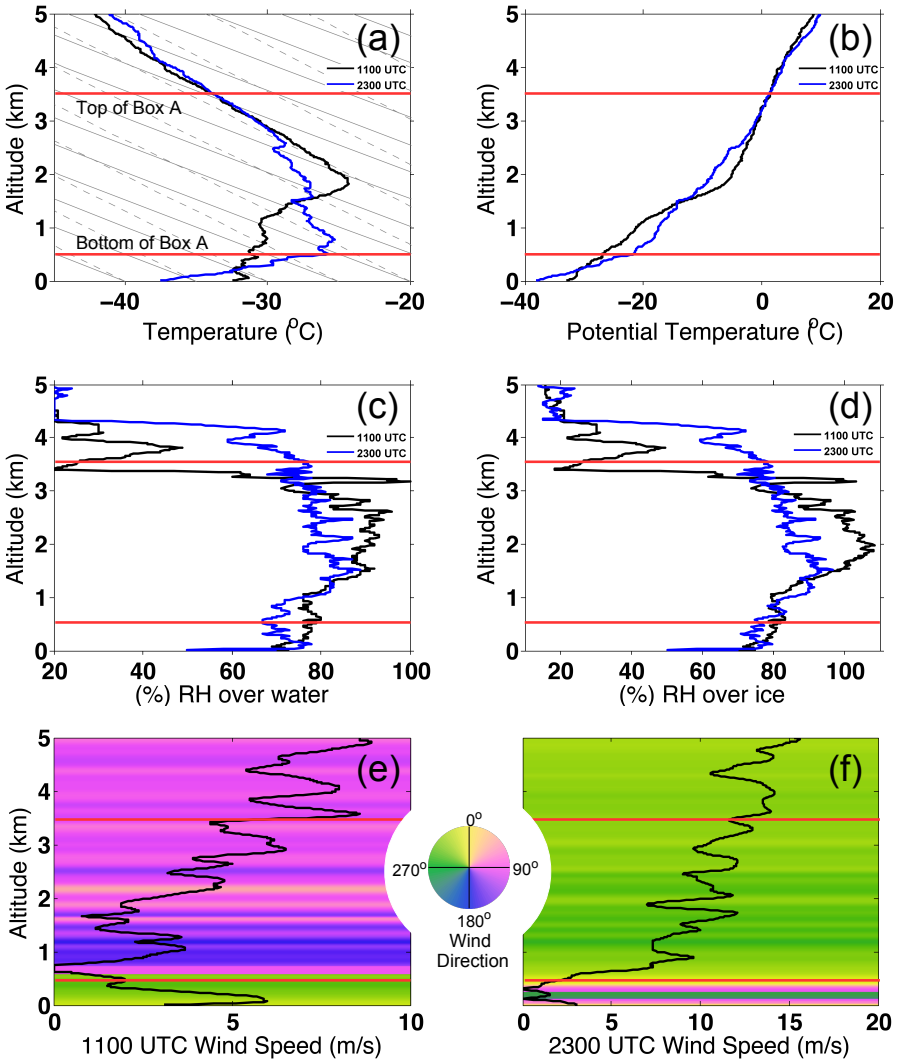

Figure 7. 14 November 2017; **(a-f)** same format as Fig. 5. Red lines show top and bottom altitudes of Box A from Fig. 6.

For Fig. 6e, the uncertainties are somewhat higher than they are for 21 March 2017 (4e) in regions of high depolarization, reaching values of 0.2 to 0.3 where $d > 0.5$. Similar to the March example, regions on 14 November 2017 in which cloud laminations are visible, namely between 10:30 and 11:00 UTC below 1 km, have absolute uncertainties smaller than 0.06 in general.

Figures 7a and b display measurements of temperature and potential temperature, respectively, from Eureka Weather Station radiosonde flights which took place at 11:00 and 23:00 UTC. The sonde data is plotted from 0 to 5 km to provide context for the plots in Fig. 6. The red lines on all Fig. 7 plots indicate the upper and lower altitude bounds of Box A from Fig. 6a, which are also the altitude bounds of Figs. 6b,c,d,e. The 23:00 UTC flight falls within the time range of Figs. 6 b,c,d,e. Dry and saturated adiabats, in solid and dashed grey, respectively, provide a guide to the thermal stability within the cloud.

Radiosonde temperatures in Fig. ~~6f~~ 7a at 11:00 UTC show a temperature inversion which begins at -32° C at the ground, increasing slowly in temperature to -30° C at 1.25 km, increasing then quite steeply to -24° C at 1.75 km (which is about the middle altitude of Figs. 6b,c,d,e). The temperature then decreases linearly to -34° C at 3.5 km (top of the small plots), and continuing the linear decrease to -43° C by 5 km. The temperature fluctuations shown by the sonde are large in the lowest altitudes, on the order of 1° C. The 23:00 UTC curve is quite different from the 11:00 UTC curve for 14 November 2017, showing an even stronger temperature inversion from -37° C at the ground to -25° C at 900 m, followed by a slow decrease to -29° C at 3 km. The temperature curve matches that from the 11:00 UTC sonde between 3 and 5 km.

The potential temperature profiles in 7b are more similar for the two sondes on this date. Both following a general increase from the ground to 5 km altitude. The slopes are slightly different for each sonde: For 11:00 UTC, potential temperature increased at a rate of 30.5° C/km for the first 550 m, then increased at a lower rate of 6.9° C/km until 5 km. The 23:00 UTC sonde found potential temperature to rise at a rate of 10.75° C/km for the first 1.2 km, which then increased to a rate of 17.9° C/km until 2 km, and then decreased to 4.8° C/km until 5 km. Between 2.75 km and 5 km the potential temperatures for both sondes are nearly identical.

Figures 7c and d give the relative humidity over water and over ice, respectively. The overall shape of the curves are quite similar for each, with the major difference being that the profiles for relative humidity over water do not exceed 100 % at any point, while the 11:00 UTC plot for relative humidity over ice does, within the altitude range of the cloud. Radiosonde relative humidity with respect to water in Fig. 7c is relatively constant with altitude for both sondes up to 1.25 km, at 70 % for 11:00 UTC and 78 % for 23:00 UTC. Over this altitude range, relative humidity over ice in Fig. ~~6g~~ 7d increases slightly from 75 % to 80 % ~~in the first 1.25 km of altitude~~ for both sondes. Unlike the ~~23~~ 21 March 2017 example, the 11:00 UTC and 23:00 UTC sondes for 14 November 2017 differ significantly above 1.25 km. For the 11:00 UTC sonde, which corresponds to the times in plots 6b,c,d,e: As the temperature ~~then~~ increases more swiftly, the relative humidity does so also, to to 90 % with respect to water, and to 107 % by 2 km ~~, decreasing back to 85~~ with respect to ice. The relative humidity over water then continues to slowly increase to 94 % at 2.75 km, while the relative humidity over ice decreases to slightly below 100 % by this altitude. An oscillating decrease is then seen in both relative humidity plots until 3 km~~. At 2.75 km altitude the relative humidity begins larger oscillations of up to 40~~ , at which point relative humidity over both water and is about 80 %~~before decreasing quickly to~~ . After a short spike to higher relative humidity values just above 3 km, both profiles then decrease immediately to

20 % by ~~3.5~~3.3 km. Above that point, relative humidity over water does not exceed 50 %, and relative humidity over ice does not exceed 45 %. The change from small to large gradients in altitude at 1.25 km is correlated with reaching the upper edge of the thicker cloud. Humidity remains high as the sonde rises through the region with lower photon count returns, and then decreases very quickly as the top of the whole cloud is reached just after 3 km.

The 23:00 UTC sonde is somewhat different. ~~The relative humidity profile begins the same way, increasing slightly from 75~~ In particular, the relative humidity values are as much as 10 % ~~to 90~~ lower over water, and 20 % ~~in the first 1.5 km. It then decreases slowly to values between 60~~ lower over ice, between 1.25 and ~~70~~ 3 km altitude, never exceeding 85 % ~~by~~ over water, nor 90 % over ice. The values are relatively constant, or slowly decreasing, up to slightly above 4 km, ~~and further still to 20 % at 4.5~~at which point a quick decrease in relative humidity is seen, which is similar to the decrease at 3 km ~~. Values at~~ in the 11:00 UTC sonde. Above 4.5 km, the response of the 11:00 UTC and 23:00 UTC ~~never exceed 90 % relative humidity~~sondes are similar. Neither the 11:00 UTC nor the 23:00 UTC profile is particularly smooth; there is lots of fine structure on the scales smaller than 100 m. Pursuing the humidity at higher resolution to match that of CRL may prove interesting, to see whether there is a correlation between the fine structure in the humidity and the laminations visible in the lidar data.

Figure 7e,f give the windspeed and direction for both sondes. The 11:00 UTC 14 November 2017 sonde is similar to the 23:00 UTC sonde from 21 March 2018: Wind direction is generally around 270° below 750 m, then shifts around toward 90° above that altitude. The wind direction in Fig. 7e is slightly more consistent at higher altitudes than it is in Fig. 5e. The windspeed stays below 9 m/s between the ground and 5 km, with a minimum at 750 m as the direction changes. The 23:00 UTC sonde on 14 November 2018 is quite similar to the 11:00 UTC sonde on that day with one wind direction below 750 m (including a bit more variability in direction for 23:00 UTC), and the opposite wind direction above that altitude. However, the directions in the 11:00 UTC and 23:00 UTC sondes are reversed with respect to each other. The windspeeds are also higher at 23:00 UTC, still generally increasing with altitude, but reaching up to 16 m/s. In the region of Figs. 7b,c,d,e, the 11:00 UTC wind profiles are relevant from 0.5 to 3.5 km. Examining Fig. 7b, a short (15 min) gap in the strong backscatter shown by the range-scaled photocounts is visible at 11:00 UTC between 1.25 km and 2.5 km, just at the time of the sonde. The laminations are far less pronounced during this gap than they are at other times of day. The sonde drifts in space during its ascent, and it takes some time for the sonde to rise. It is entirely possible that the sonde accesses some of this gap as well as other laminated parts of the cloud as it rises.

Light snow dominated the meteorological conditions reported at the ground for the first half of 14 November 2017. Hourly metorological observations recorded by the Eureka Weather Station on 14 November 2017 note snow at 00:00 UTC and 01:00 UTC, snow and blowing snow at 02:00 UTC, snow at 03:00 UTC, 04;00 UTC, and 05:00 UTC, ice crystals at 06:00 UTC, 07:00 UTC and 08:00 UTC, clear skies at 09:00 UTC, no reported condition at 10:00 UTC and 11:00 UTC, snow at 12:00 UTC through 15:00 UTC, no reported condition at 16:00 UTC and 17:00 UTC, clear skies at 18:00 UTC ,and ice crystals at 19:00 UTC, 20:00 UTC and 21:00 UTC, which are the final reports for the day. The temperature recorded at the weather station varied between -31.5° C and -38.9° C throughout the day.

4.3 ~~A summer example of layers on 26 August 2017~~

The layering seen in the Arctic clouds above CRL are not only seen during cold times of year, as in the 21 March and 14 November examples. They are also occasionally seen in summer, such as 26 August 2017. Before 04:45 UTC Fig. 11 shows optically thick low-lying clouds which are typical of summer in Eureka. Because the lidar is largely extinguished by these low clouds, we cannot discern details of any clouds above that altitude. There does appear to be some increase in signal between 3 and 4 km from 03:15 - 03:30 UTC, so it is highly likely that there are much thicker clouds above the low ones. After 04:45 UTC, we can see the full extent of some clouds which range from 0.5 to 4.5 km altitude. The same layering is present in these vertically extended clouds as we have seen in the previous examples in this paper.

26 August 2017 began with the lidar closed due to rain. Measurements were possible from 00:30 - 06:30 UTC. Despite rain being reported at the Eureka Weather Station in the hourly meteorological observations, there was so little during this time as to not impede measurements. At 06:30 UTC, the rain again became heavy enough that measurements ceased. The 355 nm laser was not operating during this measurement, so a full investigation of this case will not be presented here.

The depolarization measurements (not shown) indicate that the high-backscatter parts of the clouds before 05:00 UTC (red in Fig. 11a) have low depolarization parameter values of about 0.1, and that after 05:00 UTC the regions shown in yellow below 2 km in Fig. 11a have higher depolarization parameter of about 0.6. The interpretation is that the highly attenuating clouds early in the day are liquid, and that the precipitation which begins at 05:00 UTC consists of frozen particles. There is insufficient sensitivity in the preliminary depolarization product to determine the depolarization parameter within the layered region of the cloud after 05:00 UTC.

Hourly metorological observations recorded by the Eureka Weather Station on 26 August 2017 note cloudy conditions at 00:00 UTC, rain at 01:00 UTC, rain and fog at 02:00 UTC through 05:00 UTC, rain, snow showers and fog at 06:00 UTC, rain and snow showers at 07:00 UTC, and reports of rain and fog for the remainder of the day. The temperature recorded at the weather station varied between 0.8° C and 2.9° C throughout the day.

Fig. 11b gives the radiosonde temperature profiles, and Fig. 11c the radiosonde relative humidity profiles with respect to liquid water. The temperature profiles were very similar at 11:00 UTC and 23:00 UTC, but the relative humidity measurements differ drastically above 2.7 km. As neither sonde was launched during the CRL measurement period, we cannot draw strong conclusions from these. Still, the adiabats plotted in 11b provide a point of comparison for the temperature profiles in terms of thermal stability: On 26 August 2017, as for the other dates shown in this paper, the atmosphere was relatively stable in the region of the cloud laminations.

A summer example of fine-scale structure in clouds at Eureka. Plot of 532 nm range-scaled photocounts from 26 August 2017 **(a)**. The layers are most visible after 05:00 UTC. The measurement was stopped due to rain at 06:30 UTC. **(b, c)** give the temperature and relative humidity with respect to water from the two daily rasiosondes launched by the Eureka Weather Station. Grey solid lines in **(b)** are dry adiabats, and grey dashed lines are moist adiabats.

5 Discussion

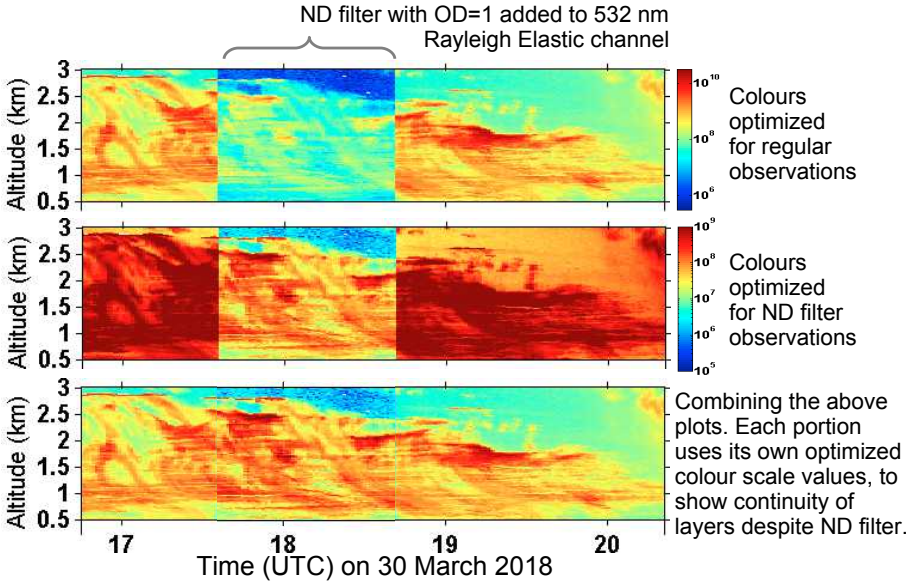

Figure 8. On 30 March 2018, during an event with the same features as previous examples, we placed an ND1 neutral density filter in front of the 532 nm Rayleigh elastic PMT for one hour. The stripes remained visible throughout the test. This is extra assurance that the PMT is not being saturated. The top panel has a colourbar which is optimized to show the stripes in the clouds before and after the ND filter test. The middle panel has a colourbar which is optimized to show the stripes during the ND filter test, when count rates were lower by a factor of about 10. The bottom panel is a combination of the first two plots. Measurements from all times during the test are shown at their own optimal colour scale so that individual layers may be identified and followed throughout the test.

~~On 30 March 2018, during an event with the same features as previous examples, we placed an ND1 neutral density filter in front of the 532 nm Rayleigh elastic PMT for one hour. The stripes remained visible throughout the test. This is extra assurance that the PMT is not being saturated. The top panel has a colourbar which is optimized to show the stripes in the clouds before and after the ND filter test. The middle panel has a colourbar which is optimized to show the stripes during the ND filter test, when count rates were lower by a factor of about 10. The bottom panel is a combination of the first two plots. Measurements from all times during the test are shown at their own optimal colour scale so that individual layers may be identified and followed throughout the test.~~

Before attributing the striped effect that we see in our data to geophysical phenomena, we apply due diligence to show that it is not an instrumental effect. Each of the topics covered by Sections 5.1- 5.4 address a specific instrumental or measurement effect/artifact which has been suggested by members of the broader lidar community as a possible indication that the laminations are not geophysical phenomena. Following that, we ~~will~~ discuss some meteorological explanations for our observations.

5.1 Ruling out PMT saturation

As discussed briefly in Section 3, the analyses are made using glued count rate profiles, which make use of photon counting signals in regions where the photon count rates are linear, and equivalent analogue signals in any region for which the photon counting rates become nonlinear. During routine processing, all regions in which the analogue signals meet or exceed the counting limits of the analogue-to-digital converter are excluded from the retrieved profiles. For all measurements in this manuscript, the PMTs were not being operated near their maximum analogue count rates, so the likelihood of the laminations being PMT saturation artifacts is low.

Further, any saturation effects should serve to smooth out the profiles at high count rates, rather than inducing the oscillating count rates as we observe as the laminated cloud phenomena. In order to ~~rule out instrumental effects associated with signal induced noise~~clearly demonstrate that these laminated features persist at much lower photon count rates, we performed a measurement with the aid of neutral density filters to lower the signal levels.

During a 30 March 2018 event which exhibited the type of layers discussed in this paper, we placed a neutral density (ND) filter with optical density 1 (ND1) in front of the 532 nm Rayleigh elastic channel's PMT. This reduces all count rates entering the PMT by a factor of 10. The ND filter was left in place for one hour, and then was removed. The results of this test are given in Fig. 8. It is clear from the composite plot in the bottom panel of Fig. 8 that the layers seen in the clouds during regular measurements (before 17:40 UTC and after 18:40 UTC) are continuous throughout the time that the ND1 filter is in place (17:40 UTC to 18:40 UTC). Since the layers are still seen at count rates which are lower by a factor of 10 compared to regular observations, we conclude that PMT saturation is not the cause of the layers.

5.2 Ruling out PMT ringing

PMT ringing effects induced by the "nonlinear response of a detector-amplifier combination to a signal larger than the dynamic range of the combination" Kovalev and Eichinger (2004) can produce phenomena in the backscattered lidar data which could, to first order, be described in a similar to the laminations seen in this manuscript: namely, vertical structures on the scale described in the manuscript. However, (a) we would not expect to see PMT ringing if the PMT is not being saturated (this has been excluded as covered in Section (5.1), above), and (b) we would expect the effects to be different than what we see in the cloud measurements.

There are several important differences between the expected ringing PMT response and the response from geophysical laminations within the clouds themselves. For a visual example of the ringing phenomenon, see Kovalev and Eichinger (2004), Figure 4.6. There, we see the "periodic nature of the returns above the cloud layer". Those backscattered returns are nearly precise repeats of the same shape as the cloud signals below. There is regular repetition as a function of range from the lidar.

On the converse, in the CRL measurements of the laminations (e.g. Figs 1, 4a, and 6a), the layers are not actually a regularly repeating pattern. They come and go, merge into one another, change in vertical extent with altitude, and are not regularly spaced in range from the lidar by any obvious geometric function.

Therefore, we do not interpret the laminated cloud features to be effects of PMT ringing.

5.3 Ruling out laser power fluctuations

Laser power fluctuations would induce increases and decreases to the range-scaled photocounts values as a function of profile number throughout the day (i.e. would manifest as vertical stripes in the plot), and cannot produce the layered features that we see in the figures, which are a function of altitude (and appear therefore as horizontal stripes in the plot).

5.4 Ruling out timing and electronics systematics

If the layers were a result of a timing offset, constant electronic noise, or similar, we might first expect the layers to be truly constant in altitude. They are not. The layers drift slowly up and down, split apart and recombine, are not always at the same altitudes, and do not always have the same individual layer thickness. Therefore we find systematic timing and electronics issues to be an unlikely source for the features displayed in the plots.

5.5 Meteorological considerations

The analysis of our measurements leads us to interpret the layered features as geophysical. Thus, the stripes in the plots are interpreted to be fine laminations within the cloud. We see these features in several types of meteorological conditions, and have seen evidence of them in more than 3 years of lidar measurements. We see them at various times of year.

Several conditions which currently seem to be associated with the laminations, and which must be taken into account when suggesting meteorological explanations, are:

1. Association with thermal/convective stability:

   The winter examples shown here exhibit a strong temperature inversion, and the summer example also has a stable temperature structure. Not all of the laminations are confined to the altitudes covered by the temperature inversion, when present.

   Radke et al. (1989) suggest, based on the work of Andraea et al. (1988), McElroy and Smith (1986) and Wakimoto and McElroy (1986), that thin, elevated, hazes can occur also at mid-latitudes and these, too, occur only in regions of great thermal stability. If the atmosphere were not vertically stable, then these laminations could not persist as they would be removed by the vertical mixing. Perhaps this is a necessary condition for such laminations. An indication to the contrary is Hobbs and Rangno (2008), which has found cloud features similar to CRL's laminated cloud layers in regions of both thermal stability and thermal instability - often within a single cloud. It is possible that the laminations form in a stable region and then drift outside that region, persisting for some time before being obliterated by vertical motions.

   Our explanations here must be consistent with stable thermal profiles, although there may exist cases of similar laminations arising in other situations.

2. Association with precipitation:

   Each case of laminated clouds shown in this paper exhibited fall streaks within the cloud, and precipitation to the ground.

We will carry out a detailed search for cases of these laminations which are and are not associated with precipitation events at the ground. It is as yet unclear whether precipitation is a necessary condition for, and/or obligatory result of, these laminations.

Explanations must allow for precipitation to the ground, since it happens in the cases shown here.

3. Association of regions of high/low range-scaled photocount rates with regions of low/high depolarization parameter:

There are regions in all plots with depolarization parameter $d < 0.1$, which indicates clear air, liquid (quasi-spherical) droplets, horizontally-oriented ice plates, or specific types of aerosols. For those $d < 0.1$ regions in which the range-scaled photocounts are high, clear air is unlikely to be the scatterer responsible; liquid droplets, oriented ice particles, and/or aerosols are more likely. Thus, our explanations must allow for the creation of, or continued existance of (if created elsewhere), liquid droplets, ice, and/or low-depolarizing aerosols.

There are certain regions in which the range-scaled photocount plots display laminations, but which are homogenous in terms of depolarization. Examples include 0.6 km to 1 km from 10:50 UTC to 11:10 UTC on 14 November 2017, and 22:00 UTC to 24:00 UTC from 1.8 km to 2.25 km on 21 March 2017.

Similarly, there are regions in which the laminations in the range-scaled count plots are less pronounced and/or absent, interrupting the consistent layered structure of the rest of the cloud. Such locations tend to have high depolarization parameter associated with high range-scaled count rates (e.g. the diagonal feature descending from 1.5 to 0.5 km from 0930 UTC to 09:50 UTC on 14 November 2017, or the smaller patch on that same day at 11:10 UTC from 0.5 to 0.6 km). Precipitating frozen particles would be consistent with this observation, and thus must not be considered to be impossible in our hypotheses.

5.6 Suggested explanations for the laminated phenomena

At this time we do not have a complete explanation of these measurements. Several explanations may be consistent with the results. Hypotheses currently under consideration include interactions with a background field of (possibly layered) aerosols, preferential condensation and/or precipitation and/or evaporation of particles, and tropospheric waves.

5.6.1 Preferential condensation and/or precipitation of particles via interaction with background field of aerosols

If we begin with a background of aerosols, perhaps already layered, in a relatively humid atmosphere, these aerosols would allow the moisture to condense upon them. Regions with more aerosols (e.g. in an aerosol layer) would be likely condensation sites, and regions with fewer aerosols (e.g. between the layers of aerosols) would not. Any existing condensed particle will scavenge remaining moisture preferentially, with larger particles growing at the expense of the nearby smaller ones and any moisture.

The larger particles at some size would become large enough to fall and precipitate out of the cloud. Any small regularity in spacing between populations of particle sizes will be exacerbated into stripes such as those we see in the presence of a very

stable atmosphere - there is no vertical mixing to disrupt the pattern. The precipitating particles should be able to fall out of the cloud without disrupting the overall layered structure.

The particles may freeze immediately upon condensation, or during precipitation. If the particles which precipitate out are frozen, and those remaining in the cloud are liquid, this would show up as bright layers with low depolarization (liquid droplets which have not yet precipitated out), and in-between regions of low brightness and higher depolarization where the few frozen particles that remain are still growing.

Many other condensation/precipitation processes are possible in this mixed-phase environment, and all should be considered when we carry out a thorough analysis. In the above situations, condensation is occurring preferentially in certain layers, and precipitation exacerbates the laminated situation.

A question then remains: What would cause the background of aerosols to have any amount of layered structure in the first place? Perhaps the explanations of Radke et al. (1984) and Radke et al. (1989) would apply. One suggested cause for morphologically-similar haze laminations is "the advection of thin hazy regions into the generally clean polar airmass and by the extreme thermal stability of the lower troposphere" (Radke et al., 1989). In Radke et al. (1984), strong windshear between haze layers and clear layers leads the authors to conclude that polluted layers of air are advected into regions of clean air, rather than a complete unit of haze layers interspersed with clean air being advected together into the region of their measurements. Further investigation of wind shear and detailed temperature structure at Eureka will be beneficial for testing this hypothesis at CRL.

5.6.2 Inhomogeneous evaporation from a uniformly condensed field

It is also possible to begin with a uniformly condensed field, and allow evaporation alone to then carry on in a non-uniform manner, leading to preferentially dried sections of the cloud. Holographic imaging results from Beals et al. (2015) demonstrate that turbulent clouds which begin with homogenous features in terms of cloud droplet number density and droplet size can become quite inhomogeneous as mixing occurs, leading to filamented structures at centimetre scales. As mixing carries on, they do not see evidence of droplets evaporating uniformly across the population (constant number density, decreasing droplet size), but instead see certain droplets evaporating entirely while the remaining droplets retain their original size (decreasing number density, constant droplet size). This mechanism could be at play within the clouds seen by CRL as well. In lidar measurements we cannot separate the droplet size from number density, as we measure a quantity proportional to a combination of these variables. Nonetheless, our observations are consistent with those of Beals et al. (2015): Regions with high number density $\times$ cross sectional droplet size, interspersed vertically with regions having low values of that quantity (and indeed being perhaps nearly free of droplets). Precipitation would still need to be accounted for (as per Section 5.5) in this scenario.

5.6.3 Persistence of layers

Persistence of the laminated cloud features measured by CRL may find its explanation in Mahrt (2014), which cites Sukoriansky and Galperin (2013): in the case of strong stratification, material can be transferred more effectively by horizontal diffusion than by vertical diffusion. This would serve to preserve any material within its own horizontal layer, rather than

spreading it out to the relatively emptier regions between the initial layers. Mahrt (2014) is focused on the boundary layer, but the turbulence theory cited applies equally to other areas of the atmosphere. Therefore the laminations in the Eureka clouds may persist due to the so-called two-dimensional quasi-horizontal) modes which are not significantly coupled in the vertical direction. Mahrt (2014) indicates that these modes can be transient, reforming and breaking down, over a variety of time scales.

5.6.4 Tropospheric waves

This hypothesis is that the laminations are the effect of gravity waves or other waves travelling through the troposphere. The waves would have a vertical wavelength of approximately 15 m (for each bright layer to be 7.5 m, and each in-between layer to also be 7.5 m). The atmosphere can sustain gravity wave motions so long as the density is decreasing with altitude. That is to say, the environmental lapse rate must be stable. Regions of adiabatic cooling will have water vapour more readily able to condense onto condensation nuclei, while the regions of adiabatic heating will be less likely to do so. Those particles which do exhibit condensation can then scavenge any surrounding moisture, as previously described, and precipitate out of the cloud. This explanation is also consistent with the layered features seeming to cease by 4 to 5 km altitude: Gravity waves are unable to continue propagating through unstable regions, which may occur at higher altitudes. Likewise, they will deposit their energy anywhere that the horizontal phase speed matches the speed of the background winds. In general, horizontal wavelengths of gravity waves tend to be much larger than the vertical wavelengths of those same waves; hence, we see finely laminated structure in the vertical (Hocking, 2001).

5.6.5 Horizontal spatial distribution of clouds

With the combining and separating of certain layers, there is also the possibility that these layers are the effect of a projection of a horizontally patchy cloud onto a measurement which is extended in time. One minute (CRL's maximum time resolution) is a long time to be watching clouds drift by if windspeeds are high, and the laser beam subtends a horizontal circle of approximate diameter 7.5 m by 5 km altitude. Further, we are interpreting a 3-D atmosphere with a 2-D measurement. Perhaps these are not contiguous layers, but rather are multiple patchy laminated clouds. With the present plots, we cannot distinguish the two situations. Understanding the horizontal spatial distribution of the observed clouds will be helpful.

5.6.6 Discussion summary

Further investigations are requisite in order to rule in or out ~~either of the~~ any of the hypotheses above, or other, possibilities. Further analysis with CRL's other channels, and Eureka's other instruments, will surely narrow down the possibilities. At the moment, we have a very intriguing phenomenon which appears to occur in frequent events at our lidar and we continue to add ancillary measurements for our next campaign.

6 Conclusions

Measurements of range-scaled photocounts at 532 nm and 355 nm, photocount ratios 532/355 nm, and 532 nm linear depolarization parameter from the CRL at Eureka, Nunavut have detected numerous instances of finely laminated cloud structures during all times of year. The individual laminations are measured to be as thin as 7.5 m per layer, with thinner features not being resolvable by CRL.

Generally, layers with high range-scaled photocount rates are associated with layers of low depolarization parameter values. Occasionally, the layered structure is interrupted by homogenous regions in terms of both range-scaled photocounts and depolarization.

The laminated clouds have, to date, only been measured during periods of precipitation reported at the ground: rain and snow. They also, for examples studied to date, seem to be associated with a stable thermal troposphere, including but not limited to days with strong temperature inversions.

This paper provides the motivation for further analysis of data sets from CRL and other high-vertical-resolution tropospheric lidars, particularly those in polar regions. The laminated cloud structures presented here are evidence that the mixed-phase clouds at Eureka are frequently not homogenous, and should not be treated as such during investigations of condensation, precipitation, and other internal microphysical processes. While the contribution of such clouds to the regional radiation budget may be precisely equal to that of homogenous clouds having the same average optical properties, it does not necessarily follow that their internal processes are identical.

Further work will be done to combine these high-resolution CRL measurement products with both low-resolution more sophisticated CRL measurement products and with high resolution measurements from other instruments at Eureka. The combination of these efforts will lead to better hypotheses and explanations for the 7.5 nm-scale features which we now know to be frequently present in Arctic clouds at Eureka.

7 Data availability

Data used in this paper available upon request from corresponding author (emccull2@uwo.ca).

Appendix A: Depolarization Uncertainty

For completeness, depolarization uncertainties for the two main dates examined in this paper are presented here. Figure 9 for 21 March 2017, and Fig. 10 for 14 November 2017.

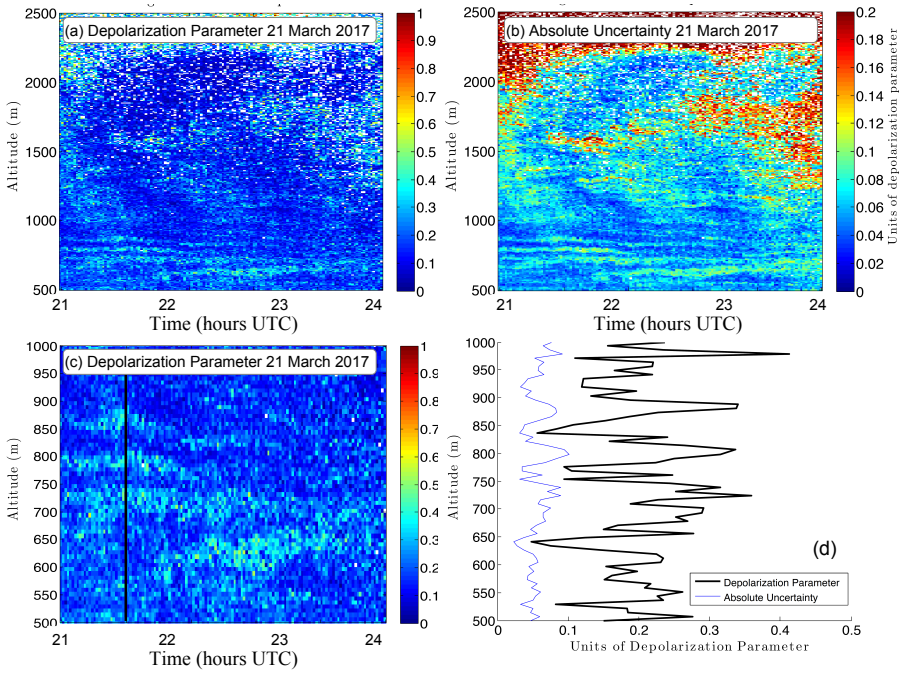

Figure 9. 21 March 2017. **(a)** is the depolarization parameter from 500 to 2500 m on a colour scale between 0 and 1. **(b)** is the corresponding absolute uncertainty in units of depolarization parameter, on a colour scale between 0 and 0.2. **(c)** is an enlarged portion of **(a)**. Black vertical line indicates the profile plotted in **(d)**. **(d)** shows a single one-minute profile of depolarization parameter in black, and its corresponding absolute uncertainty profile in blue.

Appendix B: Calculations of RH over ice

Relative humidity with respect to liquid water (RH_w) is converted to relative humidity with respect to ice (RH_i) using the Goff-Gratch formulations for saturation vapour pressure (Goff and Gratch (1946), in List (1949)). Saturation vapour pressure over water, e_w, can be calculated via equation B1:

$$\log_{10} e_w = -7.90298\left(\frac{T_s}{T}-1\right)+5.02808\log_{10}\left(\frac{T_s}{T}\right)-(1.3816\times10^{-7})(10^{11.344\left(1-\frac{T}{T_s}\right)}-1)$$
$$+(8.1328\times10^{-3})(10^{-3.49149\left(\frac{T_s}{T}-1\right)}-1)+\log_{10} e_{ws}, \quad \text{(B1)}$$

in which T is the radiosonde temperature in Kelvin, $T_s = 373.16$ K is the steam point temperature of liquid water, and $e_{ws} = 1013.246$ mb is the saturation pressure of liquid water at the steam point temperature (at 1 standard atmosphere). Saturation vapour pressure over ice, e_i, can be calculated via equation B2:

$$\log_{10} e_i = -9.09718\left(\frac{T_o}{T} - 1\right) - 3.56654\log_{10}\left(\frac{T_o}{T}\right) + 0.876793\left(1 - \frac{T}{T_o}\right) + \log_{10}(e_{io}), \tag{B2}$$

in which $T_o = 273.16$ K is the ice point temperature, and $e_{io} = 6.1071$ mb is the saturation pressure of ice at the ice-point temperature (at 0.0060273 standard atmospheres). Relative humidity with respect to ice, in percent, is then equation B3:

$$RH_i = \left(\frac{e_w}{e_{io}}\right) RH_w \tag{B3}$$

Appendix C: A summer example of layers on 26 August 2017

The layering seen in the Arctic clouds above CRL are not only seen during cold times of year, as in the 21 March and 14 November examples. They are also occasionally seen in summer, such as 26 August 2017. Before 04:45 UTC Fig. 11 shows optically thick low-lying clouds which are typical of summer in Eureka. Because the lidar is largely extinguished by these low clouds, we cannot discern details of any clouds above that altitude. There does appear to be some increase in signal between 3 and 4 km from 03:15 - 03:30 UTC, so it is highly likely that there are much thicker clouds above the low ones. After 04:45 UTC, we can see the full extent of some clouds which range from 0.5 to 4.5 km altitude. The same layering is present in these vertically extended clouds as we have seen in the previous examples in this paper.

26 August 2017 began with the lidar closed due to rain. Measurements were possible from 00:30 - 06:30 UTC. Despite rain being reported at the Eureka Weather Station in the hourly meteorological observations, there was so little during this time as to not impede measurements. At 06:30 UTC, the rain again became heavy enough that measurements ceased. The 355 nm laser was not operating during this measurement, so a full investigation of this case will not be presented here.

The depolarization measurements (not shown) indicate that the high-backscatter parts of the clouds before 05:00 UTC (red in Fig. 11) have low depolarization parameter values of about 0.1, and that after 05:00 UTC the regions shown in yellow below 2 km in Fig. 11 have higher depolarization parameter of about 0.6. The interpretation is that the highly attenuating clouds early in the day are liquid, and that the precipitation which begins at 05:00 UTC consists of frozen particles. There is insufficient sensitivity in the preliminary depolarization product to determine the depolarization parameter within the layered region of the cloud after 05:00 UTC.

Hourly metorological observations recorded by the Eureka Weather Station on 26 August 2017 note cloudy conditions at 00:00 UTC, rain at 01:00 UTC, rain and fog at 02:00 UTC through 05:00 UTC, rain, snow showers and fog at 06:00 UTC, rain and snow showers at 07:00 UTC, and reports of rain and fog for the remainder of the day. The temperature recorded at the weather station varied between 0.8° C and 2.9° C throughout the day.

Figure 12a,b give the radiosonde temperature and potential temperature profiles, and Fig. 12c,d the radiosonde relative humidity profiles with respect to liquid water and with respect to ice. The temperature profiles were very similar at 11:00 UTC

and 23:00 UTC, but the relative humidity measurements differ drastically above 2.7 km. As neither sonde was launched during the CRL measurement period, we cannot draw strong conclusions from these. Still, the adiabats plotted in 12a provide a point of comparison for the temperature profiles in terms of thermal stability: On 26 August 2017, as for the other dates shown in this paper, the atmosphere was relatively stable in the region of the cloud laminations. Figure 12e,f give the windspeed and direction for both sondes.

Author contributions. E. M. McCullough: Operation and maintenance of the lidar. Data analysis. Writing of analysis MATLAB code. Manuscript preparation. J. R. Drummond: Principal Investigator of PEARL laboratory. Contribution to manuscript preparation. T. J. Duck: Development of the CRL laboratory, and initial Principal Investigator of CRL lidar. Contribution to manuscript preparation.

Competing interests. The authors declare that they have no conflict of interest.

Acknowledgements. This research is currently supported by the Natural Sciences and Engineering Research Council, Environment and Climate Change Canada and the Canadian Space Agency.

PEARL has been supported by a large number of agencies whose support is gratefully acknowledged: The Canadian Foundation for Innovation; the Ontario Innovation Trust; the (Ontario) Ministry of Research and Innovation; the Nova Scotia Research and Innovation Trust; the Natural Sciences and Engineering Research Council; the Canadian Foundation for Climate and Atmospheric Science; Environment and Climate Change Canada (ECCC; who also provided the radiosonde data); Polar Continental Shelf Project; the Department of Indigenous and Northern Affairs Canada; and the Canadian Space Agency. This work was carried out during the Canadian Arctic ACE/OSIRIS Validation Campaigns of 2016 and 2017, which are funded by the Canadian Space Agency, Environment and Climate Change Canada, the Natural Sciences and Engineering Research Council of Canada, and the Northern Scientific Training Program. This particular project has also been supported by NSERC Discovery Grants and Northern Supplement Grants held by James R. Drummond, Robert J. Sica, and Kaley A. Walker, and the NSERC CREATE Training Program in Arctic Atmospheric Science (PI: Kim Strong).

In addition, the authors thank the following groups and individuals for their support during field campaigns at Eureka: PEARL site manager Pierre Fogal; Canadian Arctic ACE/OSIRIS Validation Campaign project lead Kaley A. Walker, CRL operators: Graeme Nott, Chris Perro, Colin P. Thackray, Jason Hopper, Shayamila Mahagammulla Gamage, and Jon Doyle; Canadian Network for the Detection of Atmospheric Change (CANDAC) operators: Mike Maurice, Peter McGovern, John Gallagher, Alexei Khmel, Paul Leowen, Ashley Harrett, Keith MacQuarrie, Oleg Mikhailov, and Matt Okraszewski; and the Eureka Weather Station staff. Thanks to Jean-Pierre Blanchet and other members of CANDAC for their helpful discussions.

References

Andraea, M. O., Browell, E. V., Garstang, M., Gregory, G. L., Harriss, R. C., Hill, G. F., and Jacob, D. J.: Biomass-burning emissions and associated haze layers over Amazonia, Journal of Geophysical Research, 93, 1509–1527, 1988.

Beals, M. J., Fugal, J. P., Shaw, R. A., Lu, J., Spuler, S. M., and Stith, J. L.: Holographic measurements of inhomogeneous cloud mixing at the centimeter scale, Science, 350, 87 – 90, 2015.

Bourdages, L., Duck, T. J., Lesins, G., Drummond, J. R., and Eloranta, E. W.: Physical properties of High Arctic tropospheric particles during winter, Atmospheric Chemistry and Physics, 9, 6881–6897, 2009.

Brock, C. A., Radke, L. F., and Hobbs, P. V.: Sulfur in particles in Arctic hazes derived from airborne in situ and lidar measurements, Journal of Geophysical Research, 95, 22 369 – 22 387, 1990.

Curry, J. A., Ebert, E. E., and Herman, G. F.: Mean and turbulence structure of the summertime Arctic cloudy boundary layer, Quarterly Journal of the Royal Meteorological Society, 114, 715–746, 1988.

Goff, J. A. and Gratch, S.: Low-pressure properties of water from -160 to 212 F, in: Transactions of the American society of heating and ventilating engineers, pp 95-122, 52nd annual meeting of the American society of heating and ventilating engineers, New York, 1946.

Hayman, M., Spuler, S., Morley, B., and VanAndel, J.: Polarization lidar operation for measuring backscatter phase matrices of oriented scatterers, Optics Express, 20, 29 553–29 567, 2012.

Hobbs, P. and Rangno, A. L.: Microstructures of low and middle-level clouds over the Beaufort Sea, Quarterly Journal of the Royal Meteorological Society, 124, 2035–2071, 2008.

Hocking, W. K.: Buoyancy (gravity) waves in the atmosphere, http://www.physics.uwo.ca/~whocking/p103/grav_wav.html, 2001.

Hoff, R. M.: Vertical structure of Arctic haze observed by lidar, Journal of Applied Meteorology, 27, 125–138, 1988.

Hogan, R. J., Francis, P. N., Flentje, H., Illingworth, A. J., Quante, M., and Pelon, J.: Characteristics of mixed-phase clouds. I: Lidar, radar and aircraft observations from CLARE'98, Quarterly Journal of the Royal Meteorological Society, 129, 2089–2116, doi:10.1256/rj.01.208, 2003.

Khattatov, V. U., Tyabotov, A. E., Alekseyev, A. P., Postnov, A. A., and Stulov, E. A.: Aircraft lidar studies of the Arctic haze and their meteorological interpretation, Atmospheric Research, 44, 99–111, 1997.

Korolev, A. V., Isaac, G. A., Strapp, J. W., Cober, S. G., and Barker, H. W.: In situ measurements of liquid water content profiles in midlatitude stratiform clouds, Quarterly Journal of the Royal Meteorological Society, 133, 1693–1699, doi:10.1002/qj.147, 2007.

Kovalev, V. A. and Eichinger, W. E.: Elastic Lidar: Theory, Practice, and Analysis Methods, John Wiley Sons, Inc., Hoboken, New Jersey, 1 edn., http://gen.lib.rus.ec/book/index.php?md5=16F1687DEAF30CDD0E02BC46D0453F58, 2004.

Lesins, G., Duck, T. J., and Drummond, J. R.: Surface energy balance framework for Arctic amplification of climate change, Journal of Climate, 25, 8277–8288, 2012.

Lindenmaier, R., Strong, K., Batchelor, R., Chipperfield, M., Daffer, W., Drummond, J., Duck, T., Fast, H., Feng, W., Fogal, P., Kolonjari, F., Manney, G., Manson, A., Meek, C., Mittermeier, R., Nott, G., Perro, C., and Walker, K.: Unusually low ozone, HCl, and HNO3 column measurements at Eureka, Canada during winter/spring 2011, Atmospheric Chemistry and Physics, 12, 3821–3835, 2012.

List, R. J.: Smithsonian Meteorological Tables, vol. 114 of *Smithsonian Miscellaneous Collections*, Smithsonian Institution Press, 4th reprint (1968) of 6th revised edn., 1949.

Loewe, K., Ekman, A. M. L., Paukert, M., Sedlar, J., Tjernström, M., and Hoose, C.: Modelling micro- and macrophysical contributors to the dissipation of an Arctic mixed-phase cloud during the Arctic Summer Cloud Ocean Study (ASCOS), Atmospheric Chemistry and Physics, 17, 6693–6704, doi:10.5194/acp-17-6693-2017, 2017.

Mahrt, L.: Stably Stratified Atmospheric Boundary Layers, Annual Review of Fluid Mechanics, 46, 23–45, 2014.

McCullough, E. M.: A new technique for interpreting depolarization measurements using the CRL atmospheric lidar in the Canadian High Arctic, Ph.D. thesis, The University of Western Ontario, London, Ontario, Canada, http://ir.lib.uwo.ca/etd/3418, 2015.

McCullough, E. M., Sica, R. J., Drummond, J. R., Nott, G., Perro, C., Thackray, C. P., Hopper, J., Doyle, J., Duck, T. J., and Walker, K. A.: Depolarization calibration and measurements using the CANDAC Rayleigh–Mie–Raman lidar at Eureka, Canada, Atmospheric Measurement Techniques, 10, 4253–4277, doi:10.5194/amt-10-4253-2017, https://www.atmos-meas-tech.net/10/4253/2017/, 2017.

McCullough, E. M., Sica, R. J., Drummond, J. R., Nott, G. J., Perro, C., and Duck, T. J.: Three-channel single-wavelength lidar depolarization calibration, Atmospheric Measurement Techniques, 11, 861–879, doi:10.5194/amt-11-861-2018, https://www.atmos-meas-tech.net/11/861/2018/, 2018.

McElroy, J. L. and Smith, T. B.: Vertical pollutant distributions and boundary layer structure observed by airborne lidar near the complex southern California coastline, Atmospheric Environment, 20, 1555–1566, 1986.

Mioche, G., Jourdan, O., Delanoë, J., Gourbeyre, C., Febvre, G., Dupuy, R., Szczap, F., Schwarzenboeck, A., and Gayet, J.-F.: Characterization of Arctic mixed-phase cloud properties at small scale and coupling with satellite remote sensing, Atmospheric Chemistry and Physics Discussions, 2017, 1–52, doi:10.5194/acp-2017-93, 2017.

Morley, B. M., Uthe, E. E., and Viezee, W.: Airborne lidar observations during AGASP-2, Journal of Applied Meteorology, 29, 268 – 271, 1990.

Morrison, H., de Boer, G., Feingold, G., Harrington, J., Shupe, M. D., and Sulia, K.: Resilience of persistent Arctic mixed-phase clouds, Nature Geoscience, pp. 11–17, 2011.

Morrison, H., de Boer, G., Feingold, G., Harrington, J., Shupe, M. D., and Sulia, K.: Resilience of persistent Arctic mixed-phase clouds, Nature Geoscience, 5, 11–17, 2012.

Nott, G., Duck, T., Doyle, J., Coffin, M., Perro, C., Thackray, C., Drummond, J., Fogal, P., McCullough, E. M., and Sica, R.: A remotely operated lidar for aerosol, temperature, and water vapor profiling in the High Arctic, Journal of Atmospheric and Oceanic Technology, 29, 221–234, 2012.

Radke, L. F., Hobbs, P. V., and Bailey, I. H.: Airborne observations of arctic aerosols III. Origins and effects of airmasses., Geophysical Research Letters, 11, 401–404, 1984.

Radke, L. F., Brock, C. A., Lyons, J. H., and Hobbs, P. V.: Aerosol and lidar measurements of hazes in mid-latitude and polar airmasses, Atmospheric Environment, 23, 2417–2430, 1989.

Ramaswamy, V. and Detwiler, A.: Interdependence of Radiation and Microphysics in Cirrus Clouds, Journal of the Atmospheric Sciences, 43, 2289–2301, 1986.

Rotermund, M., Duck, T., and Perro, C.: Characterizing the Overlap Function of the CANDAC Rayleigh-Mie-Raman Lidar in Eureka, Nunavut, in: The Connaught Summer Institute in Arctic Science, Connaught Summer Institute, 2014.

Sassen, K., Campbell, J. R., Zhu, J., Kollias, P., Shupe, M., and Williams, C.: Lidar and Triple-Wavelength Doppler Radar Measurements of the Melting Layer: A Revised Model for Dark- and Brightband Phenomena, Journal of Applied Meteorology, 44, 301–312, doi:10.1175/JAM-2197.1, https://doi.org/10.1175/JAM-2197.1, 2005.

Shupe, M., Daniel, J., de Boer, G., Eloranta, E., Kollias, P., Long, C., Luke, E., Turner, D., and Verlinde, J.: A focus on mixed-phase clouds: The status of ground-based observational methods, Bulletin of the American Meteorological Society, pp. 1549–1562, https://www.researchgate.net/profile/Pavlos_Kollias/publication/258300377_A_Focus_On_Mixed-Phase_Clouds/links/54099fa20cf2187a6a705ce6.pdf, 2008.

Solomon, A., Feingold, G., and Shupe, M. D.: The role of ice nuclei recycling in the maintenance of cloud ice in Arctic mixed-phase stratocumulus, Atmospheric Chemistry and Physics, 15, 10 631–10 643, doi:10.5194/acp-15-10631-2015, 2015.

Sotiropoulou, G., Sedlar, J., Tjernström, M., Shupe, M. D., Brooks, I. M., and Persson, P. O. G.: The thermodynamic structure of summer Arctic stratocumulus and the dynamic coupling to the surface, Atmospheric Chemistry and Physics, 14, 12 573–12 592, doi:10.5194/acp-14-12573-2014, 2014.

Sukoriansky, S. and Galperin, B.: An analytical theory of the buoyancy-Kolmogorov subrange transition in turbulent flows with stable stratification, Philosophical Transactions of the Royal Society A, 371, 2013.

Wakimoto, R. M. and McElroy, J. L.: Lidar observation of elevated pollution layers over los angeles, Journal of Climate and Applied Meteorology, 25, 1583–1599, 1986.

Zhao, X., Adams, C., Strong, K., Duck, T., Perro, C., Hudak, D., and Rodriguez, P.: Cloud identification in the Canadian High Arctic using the UV-visible colour index, in: EGU General Assembly, vol. 16, p. 13837, European Geophysical Union, Copernicus, 2014.

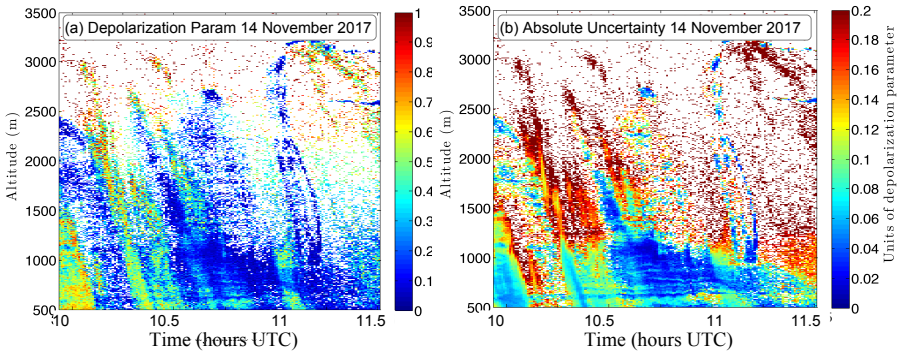

Figure 10. 14 November 2017. **(a,b)** same format as 9**(a,b)**.

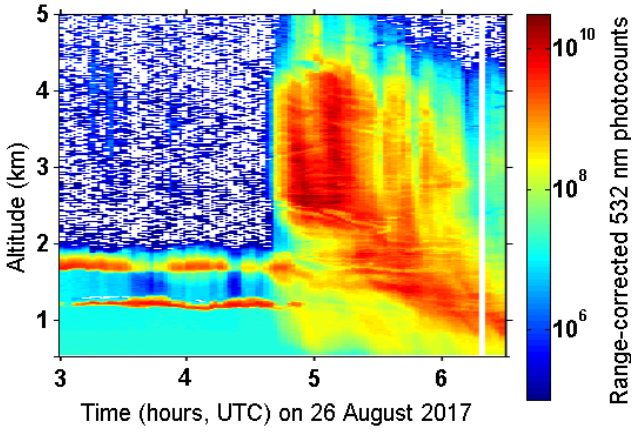

Figure 11. A summer example of fine-scale structure in clouds at Eureka. Plot of 532 nm range-scaled photocounts from 26 August 2017 **(a)**. The layers are most visible after 05:00 UTC. The measurement was stopped due to rain at 06:30 UTC.

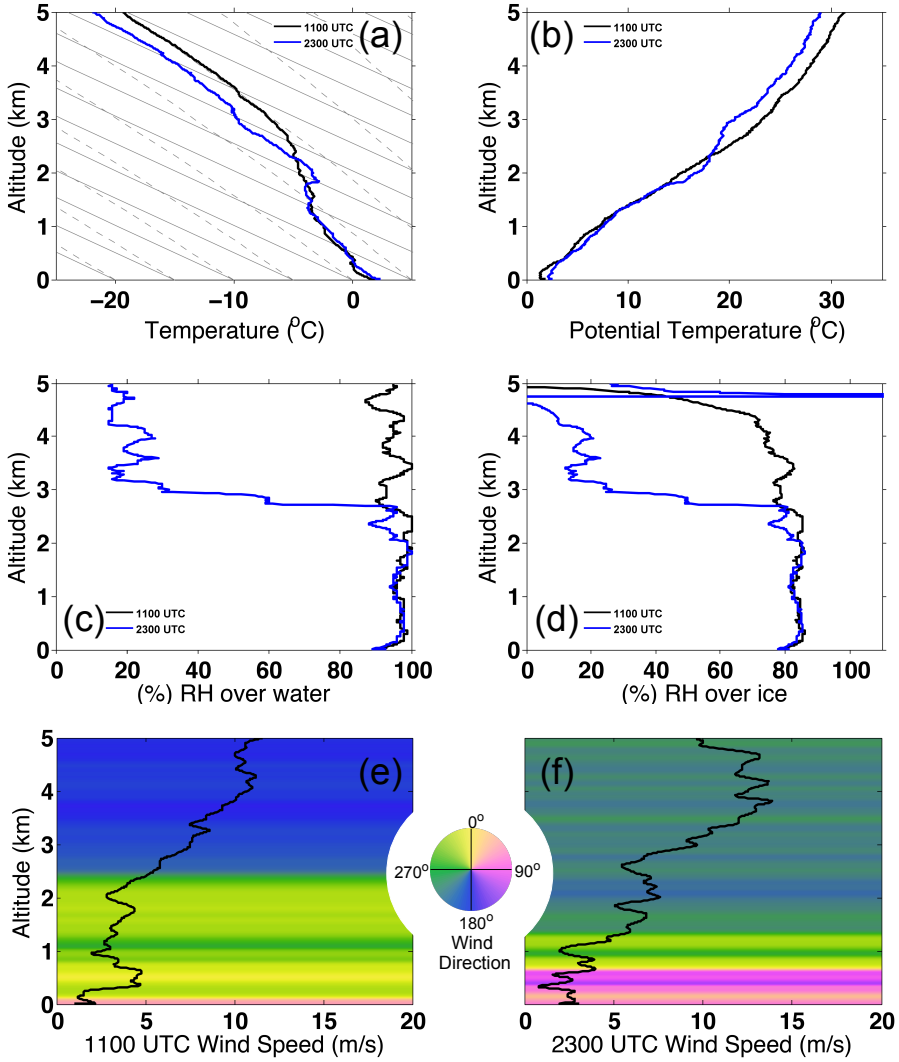

Figure 12. 26 August 2017. From the two daily rasiosondes launched by the Eureka Weather Station: **(a)** is the temperature; grey solid lines are dry adiabats, and grey dashed lines are moist adiabats. **(b)** is the potential temperature. **(c,d)** are the relative humidity with respect to water and ice respectively. **(e,f)** are the wind speed (black line) and direction (coloured background).